# Multistage Interference Cancellation with Diversity Reception for QPSK Asynchronous DS/CDMA System over Multipath Fading Channels [1]

Jianfeng Weng, Guoqiang Xue, Tho Le-Ngoc, and Sofiène Tahar

Dept. of Electrical and Computer Engineering, Concordia University

September 1998

[1]This work is partially supported by Ericsson Research Canada

**Abstract**

A new multistage interference cancellation (MIC) technique with diversity reception for QPSK asynchronous direct sequence code division multiple access (DS/CDMA) system over frequency-selective multipath Rayleigh fading channels is presented. Unlike the conventional MIC, which tries to subtract the lump sum of the multiple-access interference (MAI) and the self-interference (SI), the new MIC attempts to cancel the MAI and the partial SI, and to treat the residual SI as useful signal for symbol decision. In this technique, the Rake combining is employed so as to collect signal replicas over multiple fading paths. Upper and lower bounds for the bit error rates are derived relying on the Gaussian approximation. Further, the effect of the channel estimation error is studied. Analysis and simulation show that the new MIC can provide good performance, which is close to the ideal performance of single-user system, and outperforms the conventional MIC even in the presence of channel estimation error.

# 1 Introduction

In personal and mobile communications, direct sequence code division multiple access (DS/ CDMA) technique [1–3] has attracted considerable attention due to its potential of high capacity and its robust performance in antijam and fading channels.

In DS/CDMA system, multiple-users are allowed to simultaneously occupy a common channel to transmit the information. To distinguish the transmitted information, users are assigned distinctive signature waveforms. The signals modulated by the asynchronous users will pass through the channels and then the sum of these signals be present at the receiver. Due to the low mutual correlation between the signature waveforms, the target receiver can readily recover the information carried by the known signature waveform and treat the other users' signals as multiple access interference (MAI). In so doing, communication between the transmitter and the intended receiver can be established despite the existing multiple users' signals in the common channel. However, in such conventional demodulation scheme, the system performance may degrade when the MAI becomes strong and this results in the so-called 'near/far' problem [1]. Accordingly, the system capacity would be limited. So far, to improve the multiple-access capability, much work has been done to the alleviation of the MAI, such as the power control and the design of quasi-orthogonal signature waveforms. Unfortunately, such remedies cannot totally eliminate the 'near/far' shortcoming.

To solve the 'near/far' problem, multiuser detection has been developed ever since Verdu [4] proposed the optimum multiuser detector to achieve the minimum bit error probability in asynchronous additive white Gaussian noise (AWGN). The optimum multiuser detection is basically a maximum likelihood sequence detector consisting of a bank of matched filters followed by a Viterbi algorithm. The required complexity is on the order of O($2^K$) for $K$ active users and therefore it is undesirable for large $K$. To avoid such large computation, various efforts in designing sub-optimum multiuser detection have been conducted, such as the decorrelating detector [5], multi-stage detector [6], neural networks based detector [7], optimal bilinear detector [8], successive MAI cancellation [9], linear canceller [10], expectation maximization (EM) based iterative receiver [11], and adaptive approaches [12, 13]. A comprehensive review of the recent multi-user detectors can be found in the literature [14]. Studies indicate that although these multiuser detectors vary in complexity, they may achieve a near single user performance in AWGN channel by eliminating the MAI.

On the other hand, when the system is operating in multipath fading environment, the sum of the same information bearing signals through multiple fading paths but with different time delays and attenuation factors will be present at the receiver [1] and this results in the self-interference (SI). Therefore, apart from the MAI, the system may suffer from the SI due to the multipath propagation. To jointly suppress the MAI and the SI, the extension of the multiuser detection to the multipath fading channels has been studied [15–17]. In particular, Chen [15] studied a recursive least square (RLS) based decorrelating detector in synchronous BPSK system. Fawer and Aazhang [16] proposed a maximum-likelihood (ML) multiuser multipath detector for asynchronous BPSK and an EM based approach to solve the problem. In [17], Zvonar investigated a decorrelating approach in asynchronous BPSK and DPSK systems. Nevertheless, these detectors still require a large amount of computation especially when the numbers of active users and fading paths become large.

Among the multiuser detectors, multistage interference cancellation (MIC) [6, 9] has become a popular approach due to its simplicity and flexibility. A further interesting feature of the MIC is that it provides tentative decisions in each stage so that it can meet variable requirements of users on the bit error rate (BER). For example, for users which could tolerate high bit error rate, we may stop in the initial stage to give an acceptable BER rather than to perform many stages to achieve a very low BER. Such feature is very interesting in the future joint voice/data application [18, 19], where voice can tolerate higher bit error rates than data. In [20, 21], the extension of the MIC to asynchronous BPSK over multipath fading channel is presented, where the MIC can provide good performance by suppressing the lump sum of the MAI and the SI. It is also shown in [21] that by introducing a threshold to control the decision, a better performance can be obtained. However, no diversity technique was considered in [20, 21].

In this report, we attempt to incorporate the diversity technique (Rake combiner) in the multistage interference cancellation (MIC) and to study its performance in QPSK asynchronous DS/CDMA system over frequency-selective multipath Rayleigh fading channels. Here, QPSK is considered instead of BPSK [20, 21] due to its advantages such as its ability to achieve the same bit error probability using half the transmission bandwidth and its randomness property which renders the signal more difficult to be detected using feature detectors [1, 22]. Also, QPSK spreading scheme has been adopted in practical IS-95 CDMA digital cellular systems [22, 23]. Through the report, we will focus on QPSK phase modulation and QPSK spreading. Further, we still consider the hard symbol decision as in [20] due to the fact that the determination of an optimum threshold for the soft decision [21] is quite difficult in practice.

The MIC scheme is similar to that in [20]. In each stage of the MIC, the MAI and the SI are reconstructed relying on the tentative decisions in the previous stage and then subtracted from the received signal before the decision. Then, the Rake combiner is applied to collect the replicas from the fading paths and make symbol decision. Therefore, it is expected that the wrong tentative decisions made in the previous stage due to the detrimental effect of the interference could be corrected in the current stage and thus improve the performance.

In the study, we also found that the performance of the MIC can be further improved by simply subtracting the partial SI rather than the total SI. To elaborate this point, we may separate the SI into two parts when we reconstruct the SI part at the receiver. One is incurred by the self intersymbol interference (SII) and the other corresponds to the current symbol, henceforth to be referred to as the self current-symbol interference (SCI). It is found that the SII, behavioring like the MAI, can be effectively removed in the MIC. For the SCI, since it contains the current symbol, we may treat it as a useful signal rather than an interference so as to improve the performance. In this report, we refer to the MIC with the subtraction of the MAI and the partial SI (the SII part) as the MIC (new).

To measure the quality of the MIC (new), the ideal performance for single-user system is presented, and the upper and lower bounds for the performance in multi-user system are derived using the Gaussian approximation similarly as in [20, 21]. Also, the effect of channel estimation error on the performance of the MIC is studied. Analysis and simulation show that the MIC (new) can provide good performance close to the ideal performance of single-user system and outperforms the conventional MIC, in which the MAI and the total SI (the SII plus the SCI) are subtracted from the received signal [20, 21]. Further, even in the presence of channel estimation error, the MIC (new) still conducts better than the conventional one.

This report is organized as follows. In Section 2, we describe the asynchronous QPSK DS/CDMA system model we used together with the frequency-selective multipath fading channel model. The multistage interference cancellation scheme is presented in Section 3. Then, in Section 4, we derive the upper and lower bounds for the performances in single-user and multiuser systems. Finally, the numerical and simulation results are illustrated in Section 5 and Section 6 concludes this report.

## 2 System Description

In this report, we consider QPSK asynchronous DS/CDMA system with $K$ active users over frequency-selective multipath Rayleigh fading channels. More precisely, we consider both QPSK modulation and QPSK spreading. To give a better understanding of the system model, we describe the transmitter, the channel, the received signal, and the channel estimation models in the following.

## 2.1 Transmitter model

There are a number of techniques to configure the data modulation and the spreading modulation. For any user, if there is no restriction on the phase modulation, the balanced QPSK spreading model [22] can be used as illustrated in Fig. 1. In this figure, the binary data bits are first passing through a phase modulator and then the modulated signal, through a quadrature hybrid, is separated into two branches. Within the $n$-th symbol interval, the in-phase signal $\sqrt{\rho/N}cos(\omega_0 t - \phi_n)$ is spreaded by multiplying with the in-phase signature waveform $a^I(t)$, while the quadrature signal $\sqrt{\rho/N}sin(\omega_0 t - \phi_n)$ is spreaded by multiplying with the quadrature-phase signature waveform $a^Q(t)$, where $\omega_0$ is the carrier frequency and $\phi_n$ is an information bearing phase shift in the $n$-th symbol interval that can be taken from the set of $\{2\pi(m-1)/M, m = 1, 2, ..., M\}$ for M-PSK modulation. If QPSK phase modulation is used, then $M = 4$ [1]. Finally, the spreaded signals from two branches are summed and transmitted. By considering the symbols from $n$=$-\infty$ to $\infty$, the transmitted signal $S(t)$ can be written as

$$S(t) = \sum_{n=-\infty}^{\infty} \left[\sqrt{\rho/N}a^I(t)cos(\omega_0 t - \phi_n) - \sqrt{\rho/N}a^Q(t)sin(\omega_0 t - \phi_n)\right] P_{T_b}(t - nT_b) \qquad (1)$$

where $\rho/N$ is the signal power and $N$ is the length of the PN codes. Further, $a^I(t)$ and $a^Q(t)$ are respectively given by

$$\begin{aligned} a^I(t) &= \sum_{i=-\infty}^{\infty} a_i^I P_{T_c}(t - iT_c) \\ a^Q(t) &= \sum_{i=-\infty}^{\infty} a_i^Q P_{T_c}(t - iT_c) \qquad (2) \end{aligned}$$

where $a_i^I$ and $a_i^Q$ are respectively the in-phase and quadrature-phase pseudorandom (PN) codes taken from the set $\{-1, 1\}$. For the code length $N$, $a_i^I = a_{N+i}^I$ and $a_i^Q = a_{N+i}^Q$. $P_T(t)$ is the unit rectangular pulse of duration $T$ and $T_b$=$NT_c$.

By using the low-pass signal representation [1], $S(t)$ in (1) can be expressed in the form of

$$\begin{aligned} S(t) &= Re\left\{\sum_{n=-\infty}^{\infty}\sum_{i=-\infty}^{\infty} \sqrt{\rho/N}\left[a_i^I + ja_i^Q\right] P_{T_b}(t - nT_b)P_{T_c}(t - iT_c)e^{j(\omega_0 t - \phi_n)}\right\} \\ &= Re\left\{s(t)e^{j\omega_0 t}\right\} \qquad (3) \end{aligned}$$

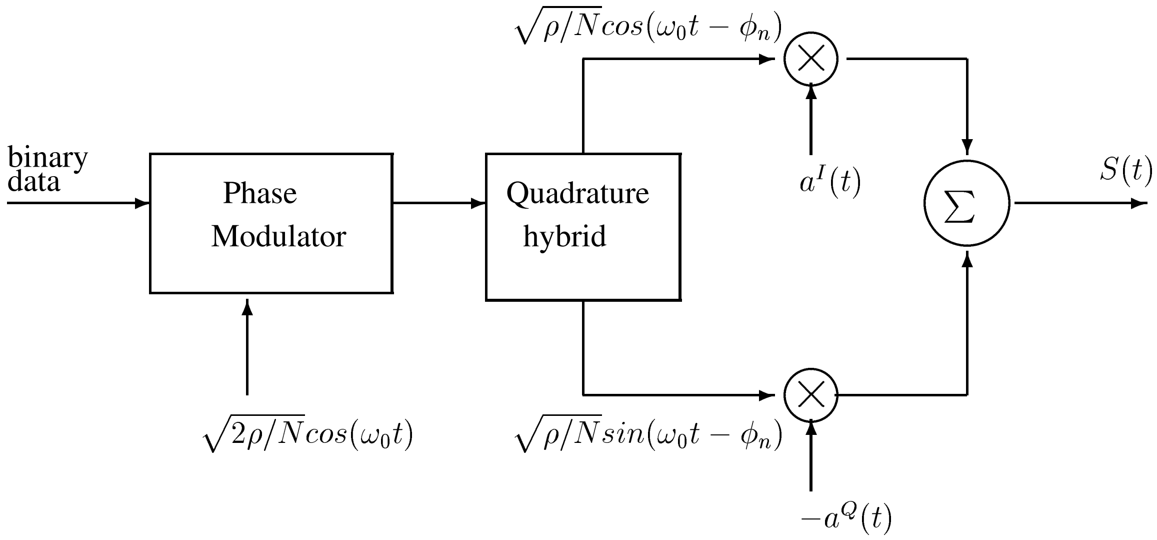


Fig. 1: Balanced QPSK transmitter model

where $s(t)$ is the equivalent low-pass signal for any user, and it can be given by

$$s(t) = \sum_{n=-\infty}^{\infty} \sum_{i=-\infty}^{\infty} \sqrt{\rho/N} \left[ a_i^I + j a_i^Q \right] e^{-j\phi_n} P_{T_b}(t - nT_b) P_{T_c}(t - iT_c) \tag{4}$$

One can readily check that when the in-phase and quadrature signature waveforms are the same, $s(t)$ in (4) simply reduces to the low-pass signal representation in [24]. Here, we consider a general case, in which the spreading is using different in-phase and quadrature signature waveforms.

When we consider multiple users in asynchronous system, we should also include the associated time delay and the phase shift for each user. Therefore, for user $k$, the transmitted signal can be written as

$$s_k(t) = \sqrt{\frac{2\rho_k}{N}} b_k(t - T^{(k)}) a_k(t - T^{(k)}) e^{j\theta_k} \tag{5}$$

where $k$ is the user index, $\rho_k := E_k/N_o$ is the normalized signal power, in which $E_k$ is the symbol energy for user $k$ and $N_o$ is the noise power spectral density. $T^{(k)}$ is the associated time delay of user $k$ that can be either random or deterministic over $[0, T_b)$. $\theta_k$ is the phase shift associated with user $k$ that can be assumed uniformly distributed over $[0, 2\pi)$. The information bearing waveform $b_k(t)$ and the signature waveform $a_k(t)$ are respectively given by

$$b_k(t) = \sum_{n=-\infty}^{\infty} e^{-j\phi_n^{(k)}} P_{T_b}(t - nT_b) \tag{6}$$

$$a_k(t) = \sum_{i=-\infty}^{\infty} \frac{1}{\sqrt{2}} \left[ a_i^{(k),I} + j a_i^{(k),Q} \right] P_{T_c}(t - iT_c) \tag{7}$$

where $\phi_n^{(k)}$ is the data bearing phase taken from the set $\{2\pi(m-1)/4, m = 1, 2, ..., 4\}$ for QPSK phase modulation. $a_i^{(k),I} = a_{N+i}^{(k),I}$ and $a_i^{(k),Q} = a_{N+i}^{(k),Q}$ are respectively the in-phase and quadrature PN codes assigned to user $k$, which are taken from the set {-1,1}. $\frac{1}{\sqrt{2}}$ is a normalization factor.

Accordingly, in asynchronous multiuser system, the equivalent low-pass signal model at the front end of the receiver can be shown in Fig. 2, where the data signals of multiple users will be modulated by the distinctive complex-valued signature waveforms $\{a_k(t - T^{(k)})\}$. After passing through the channels, the sum of multiuser signals and the background noise will be present at the receiver. In the figure, $h_k(t)$ denotes the impulse response of the channel for user $k$. In DS/CDMA system, the signal bandwidth, $W$, is usually much larger than the coherence bandwidth of the channel, $(\Delta f)_c$, and therefore the channel exhibits frequency-selective characteristic [1]. The channel model is described next.

## 2.2 Channel model

The equivalent lowpass impulse response of the channel for user $k$ can be given by (see [16, 20, 21])

$$h_k(t) = \sum_{l=1}^{L_k} \alpha_l^{(k)} \delta(t - t_l^{(k)}) \tag{8}$$

where $L_k$ is the number of paths which can be either random or deterministic. $\alpha_l^{(k)}$ and $t_l^{(k)}$ are respectively the fading parameter and the time delay in the $l$-th path of user $k$ and they are assumed mutually statistically independent for all $k$ and $l$. Let $T_m$ be the maximum channel delay spread, we note that usually $T_m \ll T_b$ (the symbol duration) [17, 21] and $t_l^{(k)} < T_m$ for all $l$ and $k$.

In (8), we assume the fading parameter $\alpha_l^{(k)}$ to be zero mean complex-valued Gaussian random variable. Further, we assume that the channel has a large coherence time, or equivalently a small Doppler spread [1], so that the fading parameter $\alpha_l^{(k)}$ exhibits a slowly changing characteristic and could be reliably estimated using a channel estimator.

## 2.3 Received signal model

From Fig. 2, the equivalent low-pass received signal, $r(t)$, can be written as

$$r(t) = \sum_{k=1}^{K} \int_{-\infty}^{\infty} h_k(\tau) s_k(t - \tau) d\tau + z(t) \tag{9}$$

where $z(t)$ is the additive white Gaussian noise(AWGN) with zero mean and unit power spectral density.

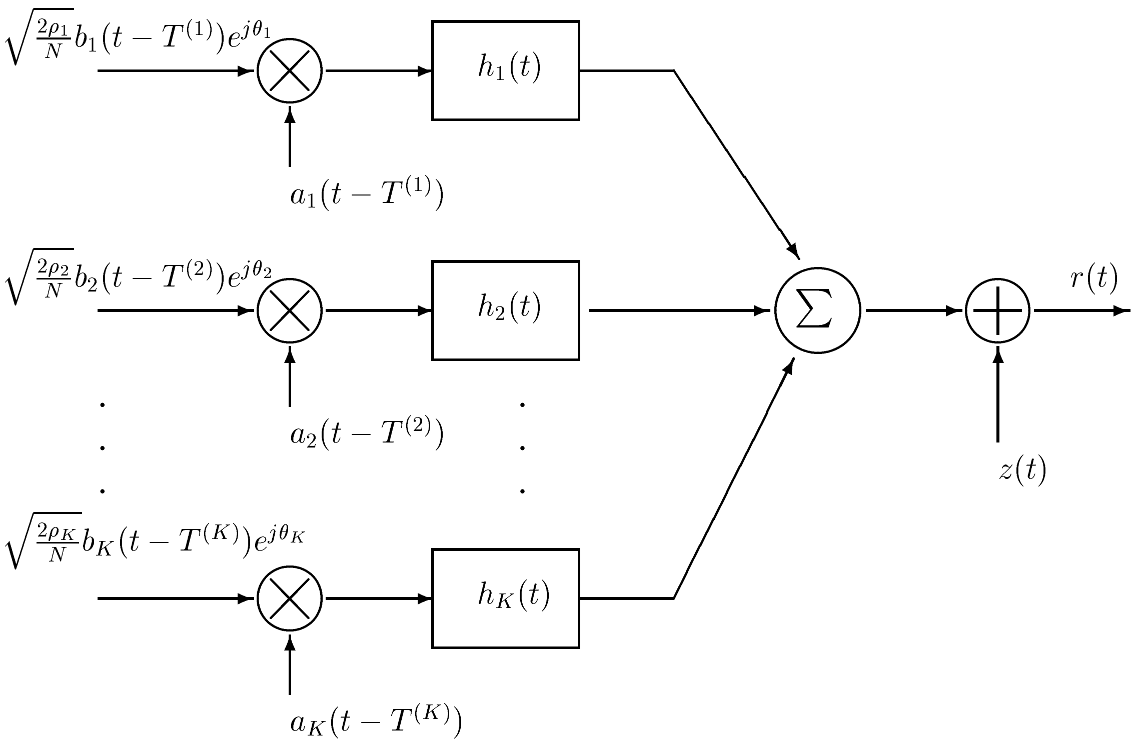


Fig. 2: Equivalent low-pass transmitter and channel model

Substituting (5) and (8) into (9) and taking the integration, we have

$$r(t) = \sum_{k=1}^{K} \sqrt{\frac{2\rho_k}{N}} \sum_{l=1}^{L_k} \alpha_l^{(k)} \, e^{j(\theta_k - \omega_0 \tau_l^{(k)})} b_k(t - \tau_l^{(k)}) a_k(t - \tau_l^{(k)}) + z(t) \tag{10}$$

where $\tau_l^{(k)} := T^{(k)} + t_l^{(k)}$, and $(\theta_k - \omega_0 \tau_l^{(k)})$ denotes the phase shift, which can be modeled uniformly distributed over $[0, 2\pi)$.

Note that in Rayleigh fading channels, $\alpha_l^{(k)}$ can be assumed to be zero-mean complex-valued Gaussian. Therefore, $\alpha_l^{(k)} e^{j(\theta_k - \omega_0 \tau_l^{(k)})}$ in the above equation is still a zero-mean Gaussian random variable. It implies that in the following the carrier phase shift part $e^{j(\theta_k - \omega_0 \tau_l^{(k)})}$ can be absorbed into $\alpha_l^{(k)}$ without loss of generality.

It is noteworthy to mention that all the models shown above are similar to those in [20, 21]. Here, however, we consider the received signals from both I and Q branches for QPSK modulation while the authors in [20, 21] only consider the received signal from the single branch (the I branch) for BPSK case.

## 2.4 Channel estimation model

Before we proceed further, it is of interest to discuss the channel estimation model due to the fact that in reconstructing the interfering signals for the interference canceller, the knowledge of the fading parameters is required [20] while in practice, such channel knowledge is usually unknown a priori and should be estimated.

The channel estimation model can be established by considering separately the estimation errors in the signal's amplitude and the carrier phase shift as in [20]. In particular, it is assumed in [20] that the estimates of the amplitude and the carrier phase shift are respectively the corresponding actual values plus Gaussian disturbance. Here, for the sake of simplicity, we consider them jointly by assuming that the estimate of the complex-valued fading parameter is the actual value plus a complex-valued Gaussian disturbance. Such consideration is also practically reasonable because the complex-valued fading parameter can be obtained via a channel estimator and the resulting estimate can be assumed Gaussian distributed [25–27]. The estimation model can be written as

$$\hat{\alpha}_l^{(k)} = \alpha_l^{(k)} + w_l^{(k)} \tag{11}$$

for all $l$ and $k$, where $w_l^{(k)}$ is the estimate noise in the $l$-th path for user $k$ and it is assumed statistically independent for all $l$ and $k$ and to be complex-valued Gaussian distributed with zero mean and variance $\sigma^2_{w_{lk}}$.

# 3 Multistage Interference Cancellation (MIC)

In this section, we will first describe the conventional Rake combiner. Then, we discuss the conventional MIC [20, 21] together with the Rake combiner. Finally, we develop the new MIC, in which only the MAI and the partial SI (the SII part) are reconstructed and subtracted from the received signal.

## 3.1 Conventional Rake combiner

At the first part of the receiver, we assume that there are $\sum_{k=1}^{K} L_k$ correlators with the waveforms $\{a_k^*(t - \tau_l^{(k)}), l = 1, 2, ..., L_k\}$ to generate the decision variables for $K$ users, where the superscript $'*'$ denotes the complex conjugate. For user $u$, the conventional Rake combiner is shown in Fig. 3. In particular, for user $u$ in the $q$-th fading path, the received signal $r(t)$ will be correlated with $\{a_u^*(t - \tau_q^{(u)})\}$ and integrated from $nT_b + \tau_q^{(u)}$ to $(n+1)T_b + \tau_q^{(u)}$. Then, the output signal will be sampled at the time instant $(n+1)T_b+\tau_q^{(u)}$. The resulting sample, denoted by $V_{n,q}^{(u)}$, is given by

$$
\begin{aligned}
V_{n,q}^{(u)} &= \frac{1}{\sqrt{N}}\int_{nT_b+\tau_q^{(u)}}^{(n+1)T_b+\tau_q^{(u)}} r(t)a_u^*(t-\tau_q^{(u)})dt \\
&= \sum_{k=1}^{K}\sqrt{2\rho_k}\sum_{l=1}^{L_k}\alpha_l^{(k)}\left[e^{-j\phi_{n-m-1}^{(k)}}R_{k,u}(\tau'_{k,l;u,q})+e^{-j\phi_{n-m}^{(k)}}\hat{R}_{k,u}(\tau'_{k,l;u,q})\right]+\eta_{n,q}^{(u)} \qquad (12)
\end{aligned}
$$

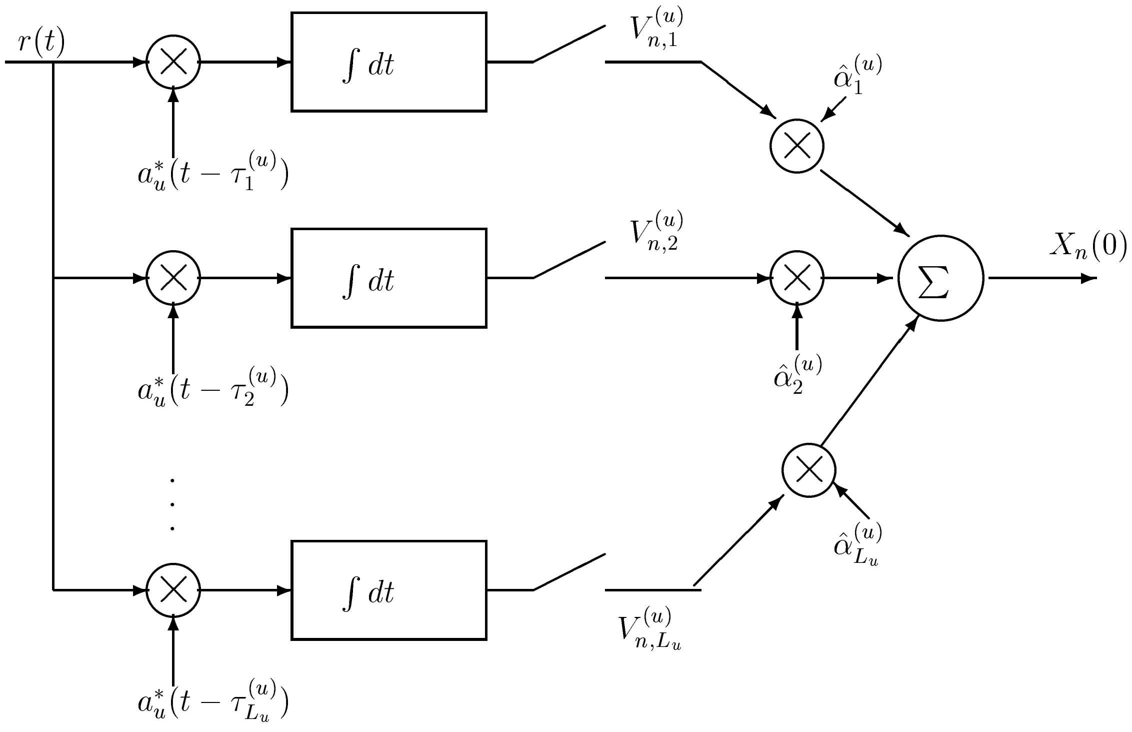


Fig. 3: Bank of correlators and the Rake combiner for user $u$

where $\frac{1}{\sqrt{N}}$ is a normalization factor, $m := \lfloor(\tau_l^{(k)}-\tau_q^{(u)})/T_b\rfloor$, and $\tau'_{k,l;u,q} := (\tau_l^{(k)}-\tau_q^{(u)})-mT_b$. $R_{k,u}(\tau)=\frac{1}{N}\int_0^{\tau}a_k(t-\tau)\,a_u^*(t)dt$ and $\hat{R}_{k,u}(\tau)=\frac{1}{N}\int_{\tau}^{T_b}a_k(t-\tau)a_u^*(t)dt$ are the partial correlation functions similarly as defined in [28] but normalized by $1/N$ and with complex-valued PN codes.

It is noteworthy to mention that in (12), the carrier phase shifts have been absorbed into $\{\alpha_l^{(k)}\}$ as mentioned previously.

In (12), $\eta_{n,q}^{(u)}$ is the noise component given by

$$
\eta_{n,q}^{(u)} = \frac{1}{\sqrt{N}}\int_{nT_b+\tau_q^{(u)}}^{(n+1)T_b+\tau_q^{(u)}} z(t)a_u^*(t-\tau_q^{(u)})dt \qquad (13)
$$

Note that $z(t)$ is the background Gaussian noise with zero mean and unit power spectral density. Hence, it can be readily shown that $\eta_{n,q}^{(u)}$ is with zero mean and unit variance. Further, by noting that for different $u$, $n$, and $q$, the integration period could be overlapped, the noise components, $\{\eta_{n,q}^{(u)}\}$, could be correlated. The covariance of $\eta_{n_1,q_1}^{(u_1)}$ and $\eta_{n_2,q_2}^{(u_2)}$ can be given by

$$\frac{1}{2}E\left\{\eta_{n_1,q_1}^{(u_1)}[\eta_{n_2,q_2}^{(u_2)}]^*\right\} = \begin{cases} 0 & \text{if } \tau_2^S > \tau_1^L \\ 0 & \text{if } \tau_1^S > \tau_2^L \\ R_{u_2,u_1}(\tau_2^L - \tau_1^S) & \text{if } \tau_1^S \le \tau_2^L \le \tau_1^L \\ R_{u_1,u_2}^*(\tau_1^L - \tau_2^S) & \text{if } \tau_2^S \le \tau_1^L \le \tau_2^L \end{cases} \tag{14}$$

where $\tau_i^S = n_i T_b + \tau_{q_i}^{(u_i)}$ and $\tau_i^L = \tau_i^S + T_b$ for $i$=1,2, and $*$ denotes the complex conjugate.

As mentioned previously, for the slowly time varying channel, the fading parameters $\{\alpha_q^{(u)}, q = 1, 2, ..., L_u\}$ can be estimated [1] and the estimation model can be given by (11). Thus, to combat fading, the Rake type combiner can be used to collect the signal replicas, i.e., $V_{n,q}^{(u)}$, over $L_u$ paths. As a result, the test statistic in the conventional Rake receiver is given by [1]

$$X_n^{(u)} = [\underline{\hat{\alpha}}^{(u)}]^H \underline{V}_n^{(u)} \tag{15}$$

where the superscript $H$ denotes the Hermitian transpose, $\underline{V}_n^{(u)} = [V_{n,1}^{(u)}, V_{n,2}^{(u)}, ..., V_{n,L_u}^{(u)}]^T$ and $\underline{\hat{\alpha}}^{(u)} = [\hat{\alpha}_1^{(u)}, \hat{\alpha}_2^{(u)}, ..., \hat{\alpha}_{L_u}^{(u)}]^T$, in which $[\cdot]^T$ denotes the transpose of $[\cdot]$.

After computing the following decision variables for QPSK ($M$=4),

$$D_p = \text{Re}\left\{X_n^{(u)}\, e^{j\psi_p}\right\} \tag{16}$$

where $\psi_p := 2\pi(p-1)/M, p = 1, 2, ..., M$, the symbol is decided in favor of

$$\hat{\phi}_n^{(u)} = \psi_p = \text{argmax}\,\{D_p\} \tag{17}$$

We can see that in the conventional Rake combiner, each user independently demodulates the received signal and then combines the replicas from multiple fading paths for symbol decision. In the detection, all other multiuser and multipath signals are treated as interference. Therefore, although this approach is quite simple, the performance of the Rake combiner would degrade due to the detrimental effect of the interferences from multiple users and multiple paths. To rescue the performance, multistage interference cancellation (MIC) [6] algorithm can be applied.

## 3.2 Conventional MIC with diversity

The MIC scheme without diversity reception over multipath fading has been addressed in [20, 21]. In the following, we would like to incorporate the Rake combining into the MIC.

To elaborate, we may rewrite $V_{n,q}^{(u)}$ of (12) into

$$V_{n,q}^{(u)} = \sqrt{2\rho_u}\alpha_q^{(u)} e^{-j\phi_n^{(u)}} + Sc_{n,q}^{(u)} + Si_{n,q}^{(u)} + M_{n,q}^{(u)} + \eta_{n,q}^{(u)} \tag{18}$$

where $Sc_{n,q}^{(u)}$, $Si_{n,q}^{(u)}$, and $M_{n,q}^{(u)}$ are respectively defined as

$$Sc_{n,q}^{(u)} = \sqrt{2\rho_u} \sum_{l=1, l\neq q}^{L_u} \alpha_l^{(u)} e^{-j\phi_n^{(u)}} \ddot{R}_{u,u}(\tau'_{u,l;u,q}) \tag{19}$$

$$Si_{n,q}^{(u)} = \sqrt{2\rho_u} \sum_{l=1, l\neq q}^{L_u} \alpha_l^{(u)} \left[ d_{m+1} e^{-j\phi_{n-m-1}^{(u)}} R_{u,u}(\tau'_{u,l;u,q}) + d_m e^{-j\phi_{n-m}^{(u)}} \hat{R}_{u,u}(\tau'_{u,l;u,q}) \right] \tag{20}$$

and

$$M_{n,q}^{(u)} = \sum_{k=1, k\neq u}^{K} \sqrt{2\rho_k} \sum_{l=1}^{L_k} \alpha_l^{(k)} \left[ e^{-j\phi_{n-m-1}^{(k)}} R_{k,u}(\tau'_{k,l;u,q}) + e^{-j\phi_{n-m}^{(k)}} \hat{R}_{k,u}(\tau'_{k,l;u,q}) \right] \tag{21}$$

where $\ddot{R}_{u,u}(\tau)$ is set to either $R_{u,u}(\tau)$ or $\hat{R}_{u,u}(\tau)$ depending on $\tau_l^{(u)} < \tau_q^{(u)}$ or not. In (20), $d_i$ is an index function which can be set to either 0 or 1 depending on $i$ equals 0 or not.

Generally speaking, the sum of $Sc_{n,q}^{(u)}$ and $Si_{n,q}^{(u)}$ is referred to as the self-interference (SI) for user $u$ while $M_{n,q}^{(u)}$ is the MAI part [20, 21]. Here, more specifically, $Sc_{n,q}^{(u)}$ is referred to as the self current-symbol interference (SCI) and $Si_{n,q}^{(u)}$ the self intersymbol interference (SII).

As shown in [20, 21], in each stage of the MIC, the MAI and the SI (both the SII and the SCI) could be reconstructed and subtracted from the received signal before the symbol decision and the resulting performance of the MIC would be much better than the conventional single-user receiver. Although the authors in [20, 21] did not mention the diversity reception, the combination of the MIC with the Rake combining is straightforward by following the approaches in [20, 21] and the Rake combining in (15). For such MIC, suppose that we are in the $i$-th stage and we have already obtained the tentative decisions in the previous stage for all interfering symbols. The output of the canceller in the $i$-th stage can be given by

$$V_{n,q}^{(u)}(i) = V_{n,q}^{(u)} - \hat{Sc}_{n,q}^{(u)}(i-1) - \hat{Si}_{n,q}^{(u)}(i-1) - \hat{M}_{n,q}^{(u)}(i-1) \tag{22}$$

where $\hat{Sc}_{n,q}^{(u)}(i-1)$, $\hat{Si}_{n,q}^{(u)}(i-1)$, and $\hat{M}_{n,q}^{(u)}(i-1)$ are the reconstructed interference parts in the $(i-1)$-th stage and they are respectively given by

$$\hat{Sc}_{n,q}^{(u)}(i-1) = \sqrt{2\rho_u} \sum_{l=1, l\neq q}^{L_u} \hat{\alpha}_l^{(u)} e^{-j\hat{\phi}_n^{(u)}(i-1)} \ddot{R}_{u,u}(\tau'_{u,l;u,q}) \tag{23}$$

$$\hat{S}i_{n,q}^{(u)}(i-1) = \sqrt{2\rho_u}\sum_{l=1,l\neq q}^{L_u}\hat{\alpha}_l^{(u)}\left[d_{m+1}e^{-j\hat{\phi}_{n-m-1}^{(u)}(i-1)}R_{u,u}(\tau'_{u,l;u,q}) + d_m e^{-j\hat{\phi}_{n-m}^{(u)}(i-1)}\hat{R}_{u,u}(\tau'_{u,l;u,q})\right] \tag{24}$$

$$\hat{M}_{n,q}^{(u)}(i-1) = \sum_{k=1,k\neq u}^{K}\sqrt{2\rho_k}\sum_{l=1}^{L_k}\hat{\alpha}_l^{(k)}\left[e^{-j\hat{\phi}_{n-m-1}^{(k)}(i-1)}R_{k,u}(\tau'_{k,l;u,q}) + e^{-j\hat{\phi}_{n-m}^{(k)}(i-1)}\hat{R}_{k,u}(\tau'_{k,l;u,q})\right] \tag{25}$$

where $\hat{\phi}_n^{(k)}(i-1)$ denotes the tentative decision of $\phi_n^{(k)}$ in the $(i-1)$-th stage for the $n$-th symbol and user $k$.

After subtracting the MAI and the SI, the Rake combining can be applied to collecting the signal replicas, i.e., $V_{n,q}^{(u)}(i)$. The output of the Rake combiner in the $i$-th stage can be given by

$$X_n^{(u)}(i) = [\underline{\hat{\alpha}}^{(u)}]^H \underline{V}_n^{(u)}(i) \tag{26}$$

where $\underline{V}_n^{(u)}(i) = [V_{n,1}^{(u)}(i), V_{n,2}^{(u)}(i), ..., V_{n,L_u}^{(u)}(i)]^T$.

Finally, as in the previous subsection, we may compute the following decision variables for QPSK ($M$=4),

$$D_p(i) = \text{Re}\left\{X_n^{(u)}(i)\, e^{j\psi_p}\right\} \tag{27}$$

where $\psi_p := 2\pi(p-1)/M, p = 1, 2, ..., M$, and then make symbol decision according to

$$\hat{\phi}_n^{(u)}(i) = \psi_p = \text{argmax}\left\{D_p(i)\right\} \tag{28}$$

For the above MIC, we now have to consider the tentative decisions in the initial stage, i.e., $i$=0. For simplicity, we let $V_{n,q}^{(u)}(0)$=$V_{n,q}^{(u)}$ and based on $V_{n,q}^{(u)}(0)$, the tentative decision $\hat{\phi}_n^{(u)}(0)$ can be readily obtained by following (26) to (28). As such, the tentative decisions made in the initial stage are equivalent to those in the conventional Rake combiner.

The above MIC scheme is similar to those in [20, 21] with the only difference that the diversity (Rake combiner) is incorporated so as to combat fading. It can be shown that such MIC can provide an improved performance over the conventional Rake combiner, to which no interference cancellation is applied.

In the above MIC, the SCI is regarded as an interference to be subtracted in (22). Nevertheless, we note that the SCI contains the current symbol, which is useful for symbol decision. As an illustration, considering the received signal in the first arriving path $V_{n,1}^{(u)}(i)$ and supposing that in the $i$-th stage, all the MAI and the SII parts have been subtracted from the received signal, we have

$$\begin{aligned} V_{n,1}^{(u)}(i) &= \sqrt{2\rho_u}\alpha_1^{(u)}e^{-j\phi_n^{(u)}} + Sc_{n,q}^{(u)} + \eta_{n,1}^{(u)} \\ &= \sqrt{2\rho_u}\alpha_1^{(u)}e^{-j\phi_n^{(u)}} + \sqrt{2\rho_u}\sum_{l=2}^{L_u}\alpha_l^{(u)}e^{-j\phi_n^{(u)}}\ddot{R}_{u,u}(\tau'_{u,l;u,1}) + \eta_{n,1}^{(u)} \end{aligned} \tag{29}$$

Now, if we disregard the received signals from other paths and assume the perfect channel knowledge, the test statisitc $X$ for the optimum demodulation is not given by $[\alpha_1^{(u)}]^* V_{n,1}^{(u)}(i)$. Rather, it would be [1]

$$X = [\beta_1^{(u)}]^* V_{n,1}^{(u)}(i) = [\beta_1^{(u)}]^* \left[\beta_1^{(u)}e^{-j\phi_n^{(u)}} + \eta_{n,1}^{(u)}\right] \tag{30}$$

where $\beta_1^{(u)} := \sqrt{2\rho_u}\alpha_1^{(u)} + \sqrt{2\rho_u}\sum_{l=2}^{L_u}\alpha_l^{(u)}\ddot{R}_{u,u}(\tau'_{u,l;u,1})$.

By using (30), the SCI part in (29) is treated as a useful signal for symbol decision rather than the interference in the SCI subtraction. In this sense, the resulting performance would be better. In the following, we modify the MIC so that in each stage of the MIC, we only reconstruct $Si_{n,q}^{(u)}$ and $M_{n,q}^{(u)}$ and then subtract them in the canceller.

## 3.3 New MIC with diversity

In this subsection, we consider the MIC with the subtraction of the MAI and the partial SI (the SII part) rather than the total SI. The Rake combining is still equipped with the MIC to collect the fading replicas. We will show that after removing the MAI and the SII, further Rake combiner can lead to an equivalent result to that obtained by the decorrelating approach for separating the multipath signals.

We still suppose that we are now in the $i$-th stage and have already obtained the tentative decisions in the $(i-1)$-th stage for all interfering symbols involved in $V_{n,q}^{(u)}$. The output of the canceller in the $i$-th stage for user $u$ is given by

$$V_{n,q}^{(u)}(i) = V_{n,q}^{(u)} - \hat{S}i_{n,q}^{(u)}(i-1) - \hat{M}_{n,q}^{(u)}(i-1) \tag{31}$$

where $\hat{S}i_{n,q}^{(u)}(i-1)$ and $\hat{M}_{n,q}^{(u)}(i-1)$ are given by (24) and (25), respectively.

Relying on $V_{n,q}^{(u)}(i)$, the tentative symbol decision for $\phi_n^{(u)}$ can be followed by (26)- (28). Further, the tentative decisions in the initial stage, i.e., $i$=0 are the same as in the conventional MIC discussed in the previous subsection, i.e., we let $V_{n,q}^{(u)}(0)$=$V_{n,q}^{(u)}$ and based on $V_{n,q}^{(u)}(0)$, we make the tentative decision $\hat{\phi}_n^{(u)}(0)$.

For illustration, we plot the structure of the new MIC with two stages in Fig. 4. The structure is shown similar to that in [20, 21]. However, due to the incorporation of diversity in the MIC, the interference cancellation for $V_{n,q}^{(u)}(i)$ has to be conducted over all the paths from $q$=1 to $L_u$ and then the Rake combiner is used to collect them before the symbol decision. Further, in each stage of the cancellation of the new MIC, the reconstruction of the SCI part is not necessary and only the MAI and the SII are reconstructed and subtracted from the received signal, while in the conventional MIC, all the MAI, the SII, and the SCI parts are reconstructed.

To gain insight of the above new MIC method, we consider a special case by assuming that all the tentative decisions in the $(i-1)$-th stage for interfering symbols are correct such that the SII part, $Si_{n,q}^{(u)}$, and the MAI part, $M_{n,q}^{(u)}$, are totally removed. The resulting signal can be written as

$$\underline{V}_n^{(u)}(i) = \mathbf{R}_s \underline{\alpha}^{(u)} \sqrt{2\rho_u} e^{-j\phi_n^{(u)}} + \underline{\eta}_n^{(u)} \tag{32}$$

where $\underline{\eta}_n^{(u)} = [\eta_{n,1}^{(u)}, \eta_{n,2}^{(u)}, ..., \eta_{n,L_u}^{(u)}]^T$.

In (32), $\mathbf{R}_s$ is an $L_u \times L_u$ correlation matrix of the signature waveforms. More precisely, its $ij$-th entry, denoted by $(\mathbf{R}_s)_{ij}$, is set to $\hat{R}_{u,u}(\tau_j^{(u)} - \tau_i^{(u)})$ if $\tau_j^{(u)} \geq \tau_i^{(u)}$ and $R_{u,u}(T_b + \tau_j^{(u)} - \tau_i^{(u)})$ otherwise. For each user, the corresponding correlation matrix $\mathbf{R}_s$ would be different. However, by the definitions for $R_{u,u}(\tau)$ and $\hat{R}_{u,u}(\tau)$ mentioned in (12), it can be shown that $\mathbf{R}_s$ for any user is a Hermitian matrix, and all the diagonal elements are one. Further, by (14), the correlation matrix of $\underline{\eta}_n^{(u)}$ can be recognized to be $\mathbf{R}_s$.

It is well-known that decorrelating operation is very useful in separating the multiuser and multipath signals [17]. Similarly, by pre-multiplying (32) with $\mathbf{R}_s$ inverse, i.e., $\mathbf{R}_s^{-1}$, the multipath signals can be separated. We have

$$\mathbf{U} = \mathbf{R}_s^{-1} \underline{V}_n^{(u)}(i) = \underline{\alpha}^{(u)} \sqrt{2\rho_u} e^{-j\phi_n^{(u)}} + \underline{w}_n^{(u)} \tag{33}$$

where $\underline{w}_n^{(u)}$=$\mathbf{R}_s^{-1} \underline{\eta}_n^{(u)}$ and $\frac{1}{2}\mathrm{E}\{\underline{w}_n^{(u)}[\underline{w}_n^{(u)}]^H\} = \mathbf{R}_s^{-1}$.

Note that in (33), the noise vector $\underline{w}_n^{(u)}$ is correlated. Thus, noise whitening approach is usually applied in order to obtain the maximal ratio combining [1, 17]. For the correlation matrix $\mathbf{R}_s$, we may let $\mathbf{R}_s = \mathbf{Q}_s \Lambda_s \mathbf{Q}_s^H$, where $\mathbf{Q}_s$ is the orthogonal matrix and $\Lambda_s = diag(\lambda_1, \lambda_2, ..., \lambda_{L_u})$ is the diagonal matrix, in which $\{\lambda_q, q = 1, 2, ..., L_u\}$ are the eigenvalues of $\mathbf{R}_s$ that are real and nonnegative [29, 30]. Next, by pre-multiplying (33) with $\Lambda_s^{\frac{1}{2}} \mathbf{Q}_s^H$ to whiten the noise vector, the output of the Rake combiner is given by

$$
\begin{aligned}
X_n^{(u)} &= \left[\Lambda_s^{\frac{1}{2}}\mathbf{Q}_s^H\underline{\hat{\alpha}}^{(u)}\right]^H \left[\Lambda_s^{\frac{1}{2}}\mathbf{Q}_s^H\mathbf{U}\right] \\
&= \left[\underline{\hat{\beta}}^{(u)}\right]^H \left[\underline{\beta}^{(u)}\sqrt{2\rho_u}e^{-j\phi_n^{(u)}} + \underline{\xi}_n^{(u)}\right]
\end{aligned} \tag{34}
$$

where $\underline{\beta}^{(u)}{:=}\Lambda_s^{\frac{1}{2}}\mathbf{Q}_s^H\underline{\alpha}^{(u)}$, $\underline{\hat{\beta}}^{(u)}{:=}\Lambda_s^{\frac{1}{2}}\mathbf{Q}_s^H\underline{\hat{\alpha}}^{(u)}$ and $\underline{\xi}^{(u)}{:=}\Lambda_s^{\frac{1}{2}}\mathbf{Q}_s^H\underline{w}_n^{(u)}{=}\Lambda_s^{-\frac{1}{2}}\mathbf{Q}_s^H\underline{\eta}_n^{(u)}$.

Equation (34) implies that the samples over $L_u$ paths in (32) can be transformed to the form of $\underline{\beta}^{(u)}\ \sqrt{2\rho_u}e^{-j\phi_n^{(u)}}$ + $\underline{\xi}_n^{(u)}$ with statistically independent noise vector $\underline{\xi}_n^{(u)}$. Note that conditioning on $\underline{\beta}^{(u)}$, $X_n^{(u)}$ in (34) is the optimum test statistic [1].

Now, if we rewrite (34) and then use (33) and (32), we obtain

$$
\begin{aligned}
X_n^{(u)} &= \left[\underline{\hat{\alpha}}^{(u)}\right]^H \mathbf{Q}_s\Lambda_s^{\frac{1}{2}} \left[\Lambda_s^{\frac{1}{2}}\mathbf{Q}_s^H\mathbf{U}\right] \\
&= [\underline{\hat{\alpha}}^{(u)}]^H\ [\mathbf{R}_s\mathbf{U}] \\
&= [\underline{\hat{\alpha}}^{(u)}]^H\ \underline{V}_n^{(u)}(i)
\end{aligned} \tag{35}
$$

The equivalence of (35) to (34) illustrates that when the SII and the MAI are totally removed, the output of the Rake combiner is equivalent to that obtained by the decorrelating operation [17]. Hence, after the subtraction of the SII and the MAI, we do not need to further adopt the decorrelating approach to separate the multipath signal because the Rake combiner inherently does. It also implies that the SCI in the new MIC is treated as a useful signal for test statistic rather than the interference. The performance of the new MIC will be evaluated in next section.

# 4 Performance analysis

In this section, we would like to evaluate the performance of the new MIC in QPSK multiuser system over multipath Rayleigh fading channels. In the analysis, we adopt the similar approach developed by Kam [31] to express the bit error rate into the form of probabilities that the test statistic falls into the wrong decision and then we apply the characteristic function to evaluate the probability [17, 32, 33]. To provide a benchmark for system performance, we first consider an ideal single-user case by ignoring all the SII and the MAI. Then, we derive the upper and lower bounds for the multi-user performance of the MIC.

In the following, the subscript $n$ and the superscript $(u)$ of $X_n^{(u)}$ are omitted whenever there is no ambiguity.

## 4.1 Ideal performance in single-user case

We assume that all the symbols are transmitted with equal probability. By ignoring the SII and the MAI, the received signal is reduced to (32) and the output of the combiner, $X$, can be expressed in either (34) or (35).

We assume that $\phi_n^{(u)}$=$\psi$ is transmitted. Thus, conditioning on $\psi$, the symbol error rate (SER) for QPSK can be written as [31, 34]

$$P_s = \sum_{p=1}^{3} A_p \tag{36}$$

where $A_p$ is the conditional probability that the Rake output multiplied with the phase shift, i.e., $X\, e^{j\psi}$ falls into the decision region $R_p$, i.e., $A_p = \Pr\{X\, e^{j\psi} \in R_p|\psi\}$ (see also Fig. 2 in [31]).

Using (34), we have

$$X\, e^{j\psi} = \left[\underline{\hat{\beta}}^{(u)}\right]^H \left[\underline{\beta}^{(u)}\sqrt{2\rho_u} + \underline{\xi}_n^{(u)} e^{j\psi}\right] \tag{37}$$

Note that $\underline{\xi}_n^{(u)}$ is a Gaussian vector and together with the phase shift $e^{j\psi}$, $\underline{\xi}_n^{(u)} e^{j\psi}$ is still a Gaussian vector with zero mean and identity covariance matrix. It implies that the conditional probability $A_p$=$\Pr\{X\, e^{j\psi} \in R_p|\psi\}$ is irrelevant to $\psi$. Therefore, in the following, we may set $\psi$=0 without loss of generality.

Usually, it is meaningful to convert the symbol error rate to the bit error rate(BER). By employing the Gray code bit mapping, we have [31]

$$P_b = (A_1 + 2A_2 + A_3)/2 = \mathcal{F}(\gamma = -\pi/4) \tag{38}$$

where $\mathcal{F}(\gamma)$:=$\Pr\{\mathrm{Re}\{X\, e^{j\gamma}\} < 0\}$ denotes the probability that the real part of $Xe^{j\gamma}$ is less than 0.

In computing $\mathcal{F}(\gamma)$, we adopt the characteristic function (CF) approach [17, 32, 33]. Letting $\Phi_\gamma(\omega)$ denote the CF of $\mathrm{Re}\{X\, e^{j\gamma}\}$, we have

$$\mathcal{F}(\gamma) = -\sum_{\{\omega_p\}} \mathrm{Res}\left[\Phi_\gamma(\omega)/\omega, \omega_p\right] \tag{39}$$

where $\{\omega_p\}$ denotes the set of poles of $\Phi_\gamma(\omega)/\omega$ in the upper half plane (Im($\omega$)>0) and $\mathrm{Res}\left[f(\omega), \omega_p\right]$ denotes the residue of $f(\omega)$ at $\omega = \omega_p$. It is noteworthy to mention that (39) is valid on the premise that $\Phi_\gamma(\omega)/\omega$ has at least a double zero at $\omega = \infty$ to allow the use of the residue theorem [32].

Next, we will evaluate $\Phi_\gamma(\omega)$. Substituting (11) into (34), we have

$$X = [\underline{\beta}^{(u)} + \Lambda_s^{\frac{1}{2}}\mathbf{Q}_s^H \Delta\underline{\alpha}^{(u)}]^H[\underline{\beta}^{(u)}\sqrt{2\rho_u} + \underline{\xi}_n^{(u)}] \tag{40}$$

where $\Delta\underline{\alpha}^{(u)}$=$\hat{\underline{\alpha}}^{(u)} - \underline{\alpha}^{(u)}$ denotes the vector of the estimate error.

Now, we let $\mathbf{R}_\beta$=$\frac{1}{2}E\{\underline{\beta}^{(u)}[\underline{\beta}^{(u)}]^H\}$. Further, by diagonalizing $\mathbf{R}_\beta$=$\mathbf{Q}_\beta\Lambda_\beta\mathbf{Q}_\beta^H$, where $\mathbf{Q}_\beta$ is the orthogonal matrix and $\Lambda_\beta$=diag($\sigma_1^2, \sigma_2^2, ..., \sigma_{L_u}^2$), where $\{\sigma_q^2, q = 1, 2, ..., L_u\}$ are the eigenvalues of $\mathbf{R}_\beta$, (40) can be written as

$$\begin{aligned} X &= [\mathbf{Q}_\beta^H\underline{\beta}^{(u)} + \mathbf{Q}_\beta^H\Lambda_s^{\frac{1}{2}}\mathbf{Q}_s^H\Delta\underline{\alpha}^{(u)}]^H[\mathbf{Q}_\beta^H\underline{\beta}^{(u)}\sqrt{2\rho_u} + \mathbf{Q}_\beta^H\underline{\xi}_n^{(u)}] \\ &= [C + G]^H[C\sqrt{2\rho_u} + Z] \\ &= C^HC\sqrt{2\rho_u} + C^H(G\sqrt{2\rho_u} + Z) + G^HZ \end{aligned} \tag{41}$$

where $C$:=$\mathbf{Q}_\beta^H\underline{\beta}^{(u)}$, $G$:=$\mathbf{Q}_\beta^H\Lambda_s^{\frac{1}{2}}\mathbf{Q}_s^H\Delta\underline{\alpha}^{(u)}$ and $Z$:=$\mathbf{Q}_\beta^H\underline{\xi}_n^{(u)}$.

We note that the elements in the vector $C$ are statistically independent, so are those in the vector $Z$. However, the elements in $G$ may be correlated and we have

$$\frac{1}{2}E\{GG^H\} = \mathbf{Q}_\beta^H\Lambda_s^{\frac{1}{2}}\mathbf{Q}_s^H\frac{1}{2}E\left\{[\Delta\underline{\alpha}^{(u)}][\Delta\underline{\alpha}^{(u)}]^H\right\}\mathbf{Q}_s\Lambda_s^{\frac{1}{2}}\mathbf{Q}_\beta \tag{42}$$

In evaluating the CF of Re $\{X\, e^{j\gamma}\}$, we first assume $\frac{1}{2}E\{GG^H\}$=$\lambda^{(G)}\mathbf{I}$. It is shown in Appendix A that the CF of Re$\{Xe^{j\gamma}\}$ can be given by

$$\Phi_\gamma(\omega) = \prod_{q=1}^{L_u}\frac{1}{a_q^2\omega^2 - 2j\omega b_q + 1} \tag{43}$$

where $a_q := \sqrt{[\lambda^{(Z)} + 2\rho_u\lambda^{(G)}]\sigma_q^2 + \lambda^{(Z)}\lambda^{(G)}}$ and $b_q := \sqrt{2\rho_u}cos\gamma\sigma_q^2$.

It is noteworthy to mention that in (43), $\lambda^{(Z)}$ actually can be set equal to 1 because we have already normalized the noise vector $Z$. Here, we still use $\lambda^{(Z)}$ instead of 1 so that (43) can be readily extended to the multi-user case as shown in the next sub-section.

Using $\Phi_\gamma(\omega)$, the bit error rate can be readily obtained via (38) and (39). Here, for the purpose of further reference, we express the BER as the function of $\lambda^{(G)}$ and $\lambda^{(Z)}$, i.e.,

$$P_b(\lambda^{(G)}, \lambda^{(Z)}) = \mathcal{F}(\gamma = -\pi/4) = -\sum_{\{\omega_p\}}\text{Res}\left[\Phi_{\gamma=-\pi/4}(\omega)/\omega, \omega_p\right] \tag{44}$$

Generally, the explicit expression of $\mathcal{F}(\gamma)$ depends on the order of the poles and is very complicated. In our case, the eigenvalues are usually distinct and thus we have

$$P_b(\lambda^{(G)}, \lambda^{(Z)}) = \sum_{q=1}^{L_u}\pi_q\frac{1}{2}\left[1 - \sqrt{\frac{b_q^2/a_q^2}{1 + b_q^2/a_q^2}}\right] \tag{45}$$

where

$$\pi_q = \prod_{l=1, l\neq q}^{L_u} \frac{1}{a_l^2\omega^2 - 2j\omega b_l + 1}\bigg|_{\omega=j(b_q/a_q+\sqrt{1+b_q^2/a_q^2})/a_q} \tag{46}$$

where $b_q := \sqrt{\rho_u}\sigma_q^2$ and $a_q$:=$\sqrt{[\lambda^{(Z)} + 2\rho_u\lambda^{(G)}]\sigma_q^2 + \lambda^{(Z)}\lambda^{(G)}}$. Note that $a_q$ is also a function of $\lambda^{(G)}$ and $\lambda^{(Z)}$.

It is noteworthy to mention that the above expression of BER is valid for both perfect and imperfect channel knowledge. In the case of perfect channel knowledge, one can readily check that by setting $\lambda^{(G)} = 0$ and $\lambda^{(Z)}$=1, (45) simply reduces to eq.14-5-28 of [1].

Now, we consider the correlated $G$. Due to the correlation of $G$ and the noise term $G^H Z$ in (41), to evaluate the CF of Re$\{Xe^{j\gamma}\}$ is quite difficult. In the following, we attempt to derive the upper and lower bounds for the BER. Note that at SNR values of practical interest, the term $G^H Z$ is relatively small in comparison with the noise term $C^H(G\sqrt{2\rho_u}+Z)$ [1, pp.275]. Hence, the upper and lower bounds for the BER are corresponding to the maximum and minimum variances of the noise $C^H G\sqrt{2\rho_u}$, respectively. Further, note that conditioning on $C$ we have $\lambda_{min}^{(G)} C^H C \leq C^H \frac{1}{2}E\{GG^H\}C$ $\leq \lambda_{max}^{(G)} C^H C$, where $\lambda_{max}^{(G)}$ and $\lambda_{min}^{(G)}$ are the maximum and minimum eigenvalues of the covariance matrix $\frac{1}{2}E\{GG^H\}$, respectively. Therefore, the upper and lower bounds for the BER can be obtained following (44) by setting $\frac{1}{2}E\{GG^H\}$ to $\lambda_{max}^{(G)}\mathbf{I}$ and $\lambda_{min}^{(G)}\mathbf{I}$, respectively. Specifically, we have

$$P_b^{(up)} = P_b(\lambda_{max}^{(G)}, 1) \tag{47}$$

$$P_b^{(low)} = P_b(\lambda_{min}^{(G)}, 1) \tag{48}$$

where $P_b(\lambda^{(G)}, \lambda^{(Z)})$ is the function defined in (44) and $\lambda^{(Z)}$ is now set to 1 because the noise vector has already been normalized. The superscripts $(up)$ and $(low)$ denote the upper and lower bounds, respectively. When the CF of Re$\{Xe^{j\gamma}\}$ has $L_u$ distinct poles, $P_b(\lambda^{(G)}, \lambda^{(Z)})$ can be evaluated via (45).

The upper and lower bounds in (47) and (48) are valid for any user but the corresponding $\mathbf{R}_s$, $\lambda_{max}^{(G)}$ and $\lambda_{min}^{(G)}$ would be different. Hence, in order to compute the bit error rate for user $k$, the evaluation of the corresponding $\mathbf{R}_s$, $\lambda_{max}^{(G)}$ and $\lambda_{min}^{(G)}$ are required. Further, in the case of perfect channel knowledge, $\lambda_{max}^{(G)}$ and $\lambda_{min}^{(G)}$ can be set to 0. Thus, $P_b^{(up)}$ and $P_b^{(low)}$ shown above are the same which represents the ideal performance of the single-user system.

## 4.2 Performance in multi-user system

### Performance in the initial stage

We first consider the multi-user performance in the initial stage ($i$=0). In the analysis, we assume that the interference terms, $Si_{n,q}^{(u)}$ and $M_{n,q}^{(u)}$, are approximately Gaussian distributed for large $K$ and $L_k$. Such approximation, although it is not exactly correct, can provide good results [20, 21]. Therefore, the analysis here is similar to those in [20, 21] but with QPSK spreading and the diversity effect.

Similarly as in the single-user case, we may assume $\phi_n^{(u)}$=0 is transmitted. We have

$$\underline{V}_n^{(u)}(0) = \mathbf{R}_s \underline{\alpha}^{(u)} \sqrt{2\rho_u} + \underline{Si}_n^{(u)} + \underline{M}_n^{(u)} + \underline{\eta}_n^{(u)} \tag{49}$$

where $\underline{Si}_n^{(u)}$:=$[Si_{n,1}^{(u)}, Si_{n,2}^{(u)}, ..., Si_{n,L_u}^{(u)}]^T$ and $\underline{M}_n^{(u)}$:=$[M_{n,1}^{(u)}, M_{n,2}^{(u)}, ..., M_{n,L_u}^{(u)}]^T$.

By using (26) and (34), the test statistic $X(0)$ can be written as

$$\begin{aligned} X(0) &= \left[\underline{\hat{\alpha}}^{(u)}\right]^H \underline{V}_n^{(u)}(0) \\ &= \left[\Lambda_s^{\frac{1}{2}} \mathbf{Q}_s^H \underline{\hat{\alpha}}^{(u)}\right]^H \Lambda_s^{-\frac{1}{2}} \mathbf{Q}_s^H \left[\mathbf{R}_s \underline{\alpha}^{(u)} \sqrt{2\rho_u} + \underline{Si}_n^{(u)} + \underline{M}_n^{(u)} + \underline{\eta}_n^{(u)}\right] \\ &= \left[\underline{\hat{\beta}}^{(u)}\right]^H \left[\underline{\beta}^{(u)} \sqrt{2\rho_u} + \Lambda_s^{-\frac{1}{2}} \mathbf{Q}_s^H (\underline{Si}_n^{(u)} + \underline{M}_n^{(u)}) + \underline{\xi}_n^{(u)}\right] \\ &= \left[\mathbf{Q}_\beta^H \underline{\hat{\beta}}^{(u)}\right]^H \left[\mathbf{Q}_\beta^H \underline{\beta}^{(u)} \sqrt{2\rho_u} + F(0) + \mathbf{Q}_\beta^H \underline{\xi}_n^{(u)}\right] \end{aligned} \tag{50}$$

where $\mathbf{Q}_\beta$ is the orthogonal matrix which diagonalizes $\mathbf{R}_\beta$ as mentioned previously, and $F(0)$:= $\mathbf{Q}_\beta^H \Lambda_s^{-\frac{1}{2}} \mathbf{Q}_s^H$ $(\underline{Si}_n^{(u)} + \underline{M}_n^{(u)})$ denotes the interference term in $X(0)$.

Similarly as in the ideal single-user case, the output of the combiner, i.e., $X(0)$, can be written as

$$X(0) = [C + G]^H \left[C\sqrt{2\rho_u} + F(0) + Z\right] \tag{51}$$

The covariance matrix of $G$, denoted by $\mathbf{R}_G$, is given by (42), while the covariance matrix of $F(0)$, denoted by $\mathbf{R}_F(0)$, can be evaluated in Appendix B. Similarly as in the previous sub-section, at SNR values of practical interest, we may ignore the term $G^H[F(0) + Z]$. Therefore, the BER is mainly determined by the noise terms $G^H C\sqrt{2\rho_u}$ and $C^H[F(0) + Z]$. Now, we let $\lambda_{max}^{(F)}(0)$ and $\lambda_{min}^{(F)}(0)$ denote the maximum and minimum eigenvalues of $\mathbf{R}_F(0)$, respectively. Thus, in deriving the upper bound for the BER, we may set $\frac{1}{2}E\{GG^H\}$=$\lambda_{max}^{(G)}\mathbf{I}$ and $\frac{1}{2}E\{F(0)F^H(0)\}$=$\lambda_{max}^{(F)}(0)\mathbf{I}$, while in deriving the lower bound for the BER, we may set $\frac{1}{2}E\{GG^H\} = \lambda_{min}^{(G)}\mathbf{I}$ and $\frac{1}{2}E\{F(0)F^H(0)\}$=$\lambda_{min}^{(F)}(0)\mathbf{I}$. As a result, the upper and lower bounds for the BER in the initial stage can be written as

$$P_b^{(up)}(0) \quad = P_b(\lambda_{max}^{(G)}, 1 + \lambda_{max}^{(F)}(0)) \tag{52}$$

$$P_b^{(low)}(0) \quad = P_b(\lambda_{min}^{(G)}, 1 + \lambda_{min}^{(F)}(0)) \tag{53}$$

The CF of Re$\{Xe^{j\gamma}\}$ can still be computed via (43) but $a_q$ is given by

$$a_q = \begin{cases} \sqrt{\left([1+\lambda_{max}^{(F)}(0)]+2\rho_u\lambda_{max}^{(G)}\right)\sigma_q^2+[1+\lambda_{max}^{(F)}(0)]\lambda_{max}^{(G)}} & \text{for} \quad P_b^{(up)}(0) \\ \sqrt{\left([1+\lambda_{min}^{(F)}(0)]+2\rho_u\lambda_{min}^{(G)}\right)\sigma_q^2+[1+\lambda_{min}^{(F)}(0)]\lambda_{min}^{(G)}} & \text{for} \quad P_b^{(low)}(0) \end{cases} \tag{54}$$

Although not specified, $\mathbf{R}_G$ and $\mathbf{R}_F(0)$ are corresponding to the user of interest. In other words, before we apply (52) and (53) to evaluate the performance for a particular user, we have evaluate the corresponding $\mathbf{R}_G$ and $\mathbf{R}_F(0)$.

**Performance in the $i$-th stage** $(i > 0)$

Due to the subtraction of the interference part, the calculation of the interference covariance matrix in the $i$-th stage $(i > 0)$ is a little bit different from that in the initial stage.

We still assume that $\phi_n^{(u)} = 0$ is transmitted. The output signal of the cancellation in the $i$-th stage is given by

$$\underline{V}_n^{(u)}(i) = \mathbf{R}_s\underline{\alpha}^{(u)}\sqrt{2\rho_u} + \underline{\tilde{S}i}_n^{(u)}(i-1) + \underline{\tilde{M}}_n^{(u)}(i-1) + \underline{\eta}_n^{(u)} \tag{55}$$

where $\underline{\tilde{S}i}_n^{(u)}(i-1)$=$[\tilde{S}i_{n,1}^{(u)}(i-1), \tilde{S}i_{n,2}^{(u)}(i-1), ..., \tilde{S}i_{n,L_u}^{(u)}(i-1)]^T$, $\underline{\tilde{M}}_n^{(u)}(i-1)$=$[\tilde{M}_{n,1}^{(u)}(i-1), \tilde{M}_{n,2}^{(u)}(i-1), ..., \tilde{M}_{n,L_u}^{(u)}(i-1)]^T$, $\tilde{S}i_{n,q}^{(u)}(i-1)$:=$Si_n^{(u)}$-$\hat{S}i_n^{(u)}(i-1)$, and $\tilde{M}_n^{(u)}(i-1)$:= $M_n^{(u)}$ - $\hat{M}_n^{(u)}(i-1)$.

Due to the fact that in each stage, the test statistics for all users are correlated and thus the tentative decisions for all interfering symbols in the $(i-1)$-th stage, $\{\hat{\phi}_n^{(k)}(i-1)\}$, are correlated and dependent on the fading parameters $\{\alpha_l^{(k)}\}$ and the noise components $\{\eta_{n,q}^{(k)}\}$, the performance evaluation in the $i$-th stage $(i > 0)$ is even more complicated. One possible approach is to compute the bit error rate conditioning on all $\{\alpha_l^{(k)}\}$ and then take the ensemble average [33]. However, it requires an excessive computational effort especially in evaluating the high dimensional numerical integration. Here, by using the well-designed PN codes, we assume that $\{\hat{\phi}_n^{(k)}(i-1)\}$ are weakly correlated and the residual interference is approximately Gaussian distributed as in [20, 21]. Accordingly, following the approach in the initial stage, the upper and lower bounds for the BER can be evaluated relying on the covariance matrix of the interference vector $F(i)$:=$\mathbf{Q}_\beta^H\Lambda_s^{-\frac{1}{2}}\mathbf{Q}_s^H[\underline{\tilde{S}i}_n^{(u)}(i-1) + \underline{\tilde{M}}_n^{(u)}(i-1)]$.

Let $\mathbf{R}_F(i)$ denote the covariance matrix of $F(i)$. From (55), we note that the evaluation of $\mathbf{R}_F(i)$ is dependent on the bit error rate in the previous stage $(i-1)$, of which the exact result is unfortunately difficult to be obtained and the upper and lower bounds are derived. Therefore, we further let $\mathbf{R}_F^{(up)}(i)$ denoting the covariance matrix of $F(i)$ evaluated from $P_b^{(up)}(i-1)$ and $\mathbf{R}_F^{(low)}(i)$ the one evaluated from $P_b^{(low)}(i-1)$. In Appendix C, the evaluation of $\mathbf{R}_F^{(up)}(i)$ and $\mathbf{R}_F^{(low)}(i)$ is given. It is noteworthy to mention that for different users, the corresponding $P_b^{(up)}(i-1)$ and $P_b^{(low)}(i-1)$ are different. Therefore, in order to evaluate $\mathbf{R}_F^{(up)}(i)$ and $\mathbf{R}_F^{(low)}(i)$, all $P_b^{(up)}(i-1)$ and $P_b^{(low)}(i-1)$ for interfering users involved in $F(i)$ have to be evaluated.

Next, letting $\lambda_{max}^{(F,up)}(i)$ denote the maximum eigenvalue of $\mathbf{R}_F^{(up)}(i)$ and $\lambda_{min}^{(F,low)}(i)$ the minimum eigenvalue of $\mathbf{R}_F^{(low)}(i)$, we may set respectively $\frac{1}{2}E\{F(i)F^H(i)\}$ to $\lambda_{max}^{(F,up)}(i)\mathbf{I}$ and $\lambda_{min}^{(F,low)}(i)\mathbf{I}$ in computing the upper and lower bounds of the BER in the $i$-th stage. We hence have

$$P_b^{(up)}(i) \quad = P_b(\lambda_{max}^{(G)}, 1+\lambda_{max}^{(F,up)}(i)) \tag{56}$$

$$P_b^{(low)}(i) \quad = P_b(\lambda_{min}^{(G)}, 1+\lambda_{min}^{(F,low)}(i)) \tag{57}$$

As in section 4.2.1, the CF of Re$\{Xe^{j\gamma}\}$ can still be evaluated via (43) but $a_q$ is given by

$$a_q = \begin{cases} \sqrt{\left([1+\lambda_{max}^{(F,up)}(i)] + 2\rho_u\lambda_{max}^{(G)}\right)\sigma_q^2 + [1+\lambda_{max}^{(F,up)}(i)]\lambda_{max}^{(G)}} & \text{for} \qquad P_b^{(up)}(i) \\ \sqrt{\left([1+\lambda_{min}^{(F,low)}(i)] + 2\rho_u\lambda_{min}^{(G)}\right)\sigma_q^2 + [1+\lambda_{min}^{(F,low)}(i)]\lambda_{min}^{(G)}} & \text{for} \qquad P_b^{(low)}(i) \end{cases} \tag{58}$$

As mentioned in the previous subsection, before we apply (56) and (57) to evaluate the performance for a particular user, we have evaluate the corresponding $\mathbf{R}_G$ and $\mathbf{R}_F(i)$.

The numerical and simulation results are presented in next section to illustrate the performance of the MIC.

# 5 Numerical and simulation results

In this section, we present several numerical and simulation results for the BER of the MIC with diversity in QPSK asynchronous CDMA system over multipath Rayleigh fading channels. Without loss of generality, we assume that the first user is the user of interest.

## 5.1 System model

In the study, we consider identical fading channels by setting E$\{[\alpha_l^{(k)}]^2\} = 2$ for all fading paths. Obviously, we have $\mathbf{R}_\alpha = \mathbf{I}$. It is noteworthy to mention that our analysis is valid for arbitrary $\mathbf{R}_\alpha$ and applicable to unbalanced fading channels. For user $k$, the total SNR$\#k$ per bit over the $L_k$ fading channels is set to $\frac{1}{2}L_k2\rho_k$E$\{[\alpha_l^{(k)}]^2\}/log_2M$=$\rho_kL_k$, where $log_2M$ is a factor used to obtain the SNR per bit. Further, we assume that the number of paths, $L_k$, is the same for all users and is denoted by

$L$. Gold sequences with $N$=31 are considered as the PN codes, where the $m$-sequences for generating Gold sequences are represented in octal by 45 (11001) and 67 (00011). Here the sequences in the brackets are the corresponding initial AO/LSE loadings [35]. It is noteworthy to mention that for any user, a pair of Gold sequences is assigned as the in-phase and quadrature PN codes. For any user, say user $k$, the time delay associated with the fading path, $t_l^{(k)}$, is set to $lT_c/2$ so that $h_k(t)$ in (8) is equivalent to the tapped delay-line multipath fading model with time spacing $T_c/2$ [1], while the time delay associated with user $k$, $T^{(k)}$, is set to $(k-1)T_b/10 \ mod \ T_b$ for $N$=31, where without loss of generality $T^{(k)}$ is arranged within $[0, T_b)$. The total time delay for user $k$ in the $l$-th path is $\tau_l^{(k)}$=$T^{(k)}$+$lT_c/2$.

In the simulation, we need to generate the received samples $V_{n,q}^{(u)}$, the fading parameters, and the background Gaussian noises $\{\eta_{n,q}^{(u)}\}$ in (12) for $q$=1,2,...,$L$ and $u$=1,2,...,$K$. Due to the possible correlation of the noise components $\{\eta_{n,q}^{(u)}\}$ as mentioned in (13) and (14), to generate $\{\eta_{n,q}^{(u)}\}$ symbol by symbol is quite difficult. Therefore, we proceed the simulation trials as follows. In each trial, we generate a sequence of received samples $V_{n,q}^{(u)}$ for $q$=1,2,...,$L$ and $u$=1,2,...,$K$ from $n = n_o$ to $n = n_o + P - 1$, where $P$ is the sequence length and $n_o$ is a particular starting index. During the period from $n = n_o$ to $n = n_o + P - 1$, the correlation of the noise components can be computed via (13) and (14). Thus, letting $\mathbf{R}_\eta$ denote the covariance matrix of these noise components, we may generate the correlated $\{\eta_{n,q}^{(u)}\}$ by multiplying the square root matrix of $\mathbf{R}_\eta$ with a sequence of white Gaussian noise samples. On the other hand, for the fading parameters, to reflect the statistically Rayleigh fading channel, the fading parameters of all users over $L$ fading paths will be randomly generated from sequence to sequence such that their amplitudes are Rayleigh distributed. Within each period from $n = n_o$ to $n = n_o + P - 1$, however, these fading parameters will be maintained unchanged.

The selection of the sequence length $P$ is based on the number of stages in the MIC due to the partial intersymbol interference. Specifically, in making the current symbol decision for a particular user, the MIC may have to estimate the tentative decisions in the previous stage for the two consecutive interfering symbols of other users (see (31) and Fig. 4). In other words, if we consider the symbol decision in the $S$-stage of the MIC, the number of involved interfering symbols in the initial stage would be at least $2S$. Therefore, in our simulation, we set the sequence length $P$ to $2S + 3$ to make sure all the involved symbols are taken into consideration. Further, in the $S$-stage MIC, the symbol decision will be made for the $(S+1)$-th symbol in this sequence. In our case, since we wish to evaluate the performance of the MIC in the second stage, $S$ is set to 2 through all the following simulation.

Relying on the received samples generated above, we will compare the simulated performances of the new MIC, the conventional MIC, and the conventional Rake receiver. The output of the canceller for the new MIC in the $i$-th stage ($i > 0$) is given by (31), where apart from the MAI, only the partial SI, i.e., $\hat{S}i_{n,q}^{(u)}$, rather than the total SI is subtracted. On the other hand, the $i$-th stage canceller output for the conventional MIC is given by (22), where the SCI, the SII and the MAI are subtracted. For simplicity, the conventional MIC is referred to as the MIC (old). In both MICs, the decision in the $i$-th stage is made according to (26)-(28). We let MIC-$i$ denote the MIC performance which relies on the $i$-th stage decision. Besides, noting that the test statistic in the initial stage of both MICs is the same to that in the conventional Rake receiver, where no interference cancellation is applied, we will use the MIC-0 to represent the conventional Rake receiver in the following. Finally, the symbol decisions will be compared with the actually transmitted symbol to compute the error events of bits.

The analytical bounds for the BER can be evaluated using the formulae in the previous section, while the simulated BER is estimated from $3 \times 10^6$ Monte Carlo trials. All the numerical evaluation and the Monte Carlo simulation are conducted via a C program while the involved matrix decompositions and the square root matrix of $\mathbf{R}_\eta$ are calculated using the MATLAB software.

It is noteworthy to mention that instead of introducing a threshold for soft decision as in [21], we focus on the hard decision in the MIC due to the fact that the determination of the optimum threshold is practically complicated.

## 5.2 Results

We first consider the performance in the case of perfect channel knowledge. Accordingly, in the theoretical analysis, we may set $\lambda^{(G)}$=0.

### Performance vs. SNR

The BER for the MIC in a 3-user system over 2-path Rayleigh fading channels is plotted versus SNR in Fig. 5 for $N$=31. All users are considered with equal power. In the figure, the single-user performance is evaluated via either (47) with $\lambda_{max}^{(G)}$=0 or (48) with $\lambda_{min}^{(G)}$=0 due to the perfect channel knowledge. The other BERs are obtained from the simulation. It can be seen that both the MIC (new) and the MIC (old) with $i > 0$ can provide significant performance improvement over the conventional Rake receiver (MIC-0), in which no interference cancellation scheme is used. Further, by increasing the number of stages from MIC-1 to MIC-2, the performance improvement is negligible while by using the new MIC instead of the old one (MIC (old)), the BER can be further decreased and a near single-user performance achieved. In particular, at the BER level of $10^{-3}$, approximately 2dB performance improvement in SNR can be achieved by the MIC (new) over the MIC (old).

In Fig. 6, we compare the analytical and simulation results on the BER of the MIC (new) versus SNR in a 3-user system with $N$=31 over 2-path Rayleigh fading channels. We are still considering the equal power for all users. The BERs of the MIC-0,1,2 are obtained via simulation, while the upper and lower bounds for the MIC-0 are evaluated respectively via $P_b^{(up)}(0)$ and $P_b^{(low)}(0)$ in (52) and (53), and the upper bounds for the MIC-1,2 are obtained via (56). In the evaluation, the eigenvalue of $\mathbf{R}_G$ is set to zero. The lower bounds for the MIC-1,2 are not plotted due to the fact that they are very close to the single-user curve in the 3-user case. It can be seen that the simulation results of the MIC-0,1,2 are well upper bounded by the analytical results. The upper bound is shown tight for low SNR values but loose for high ones especially in the case of the MIC-1. Our explanation for this is as follows. From (56), where $\lambda_{max}^{(G)}$ is set to 0 because of the perfect channel knowledge, we note that given $\rho_u$ and $\sigma_q^2$, the maximum eigenvalue of the covariance matrix of the residual interference, i.e., $\lambda_{max}^{(F,up)}(i)$, mainly determines the upper bound. It is shown in Appendix C that in computing the covariance matrix, we adopt the worst case BER in the previous stage (MIC-0). This may result in some performance gap. On the other hand, for high SNR values, the interference part can be effectively removed such that the residual interference may not be well approximated by Gaussian distribution. Hence, when the Gaussian approximation is adopted in the analysis, the results may deviate from the simulation.

**Effect of number of users**

The simulation results on the BER of the MIC versus the number of users ($K$) at SNR=20dB over 2-path Rayleigh fading channels are plotted in Fig. 7. All users are with equal power. It can be seen that as $K$ increases, the performances of both the MIC-1 (new) and the MIC-1(old) are degraded. To rescue the performance, the 2-stage MIC (MIC-2) appears necessary especially when $K$ is large ($K > 7$). Further, the results show that the MIC (new) still outperforms the MIC (old). Specifically, if we set BER=$10^{-3}$ as an acceptable performance level, the system can accommodate 8 active users by using the MIC-1 (old) while it can further accommodate 2 additional users by using the MIC-1 (new). Moreover, when the MIC-2 is used, both the MIC-2 (new) and the MIC-2 (old) can accommodate at least 12 users but the MIC-2 (new) provides better performance. In contrast, when we use the conventional Rake combiner (MIC-0), where no interference cancellation is applied, the system can approximately tolerate 2 users.

The corresponding upper and lower bounds for the MIC (new), evaluated via (56) and (57), respectively, at SNR=20dB over 2-path Rayleigh fading channels are shown in Fig. 8, from which it can be seen that generally the simulation results are well bounded by the analytical ones. It appears that although the Gaussian approximation adopted in analysis is not exactly true, it may provide good performance reference. However, we also note that some simulation results are shown slightly lower than the analytical lower bound. Such phenomenon may be due to the approximation used in the theoretical analysis and the accuracy of the simulation results.

**Effect of interfering powers**

Fig. 9 plots the simulated BER of the MIC versus the SNR$\#$3-SNR$\#$1 in 3-user system at SNR$\#$1= 20dB over 2-path fading channels, where SNR$\#$2= (SNR$\#$3+SNR$\#$1)/2dB. As shown in the figure, the performance of the MIC-1,2 (old) is much better than that of the MIC-0 due to the subtraction of the MAI and the SII. However, it is also shown that the performance of the MIC-1,2 (old) unfortunately degrades slightly as SNR$\#$3 and SNR$\#$2 become large. A possible explanation for this is that as SNR$\#$3 and SNR$\#$2 become large, the probability of making a wrong tentative decision for user $\#$1 would increase and thus when the MIC (old) subtracts the SCI part, which involves the tentative decision of user $\#$1, the performance degradation will occur. It appears that the subtraction of the SCI in the MIC-1,2 (old) cannot improve but worsen the performance. In contrast, the performance of the MIC-1,2 (new) is shown almost insensitive to the powers of interfering users. Through the results, it can be inferred that the MIC (new) can tolerate the imperfect power control while the MIC (old) may still suffer from the non-ideal power control.

**Effect of number of diversities**

In Fig. 10, the analytical and simulated BERs of the MIC versus the number of diversities ($L$) in 3-user system at SNR=20dB and $N$=31 over multipath Rayleigh fading channels are plotted, where $L$ is also the number of fading paths. It is assumed that the receiver knows the number of paths so that $L$ diversities can be applied to the case of $L$ paths. All users are with equal power. The results show that with the increase of $L$, the MIC-1 (new) provides significant performance improvement over the MIC-1 (old) and the conventional Rake (MIC-0). This is possibly due to the fact that the

MIC-1 (new) treats the self current interference (SCI) as signal while the MIC-1 (old) regards it as the interference. In the case of $L$=1 (no self interference), there is no performance between the MIC (new) and the MIC (old) because these two schemes are the same when there is no self interference. For large $L$ (more SCI), however, the performance difference would be salient. From the figure, we also note that the simulation results of the MIC-1 (new) are well bounded by the analytical results. However, the analytical bounds will be much looser for the MIC-0 as $L$ becomes large because there would be more self interference in the initial stage. It is noteworthy to mention that for $L$=1, the upper and lower bounds merge to be one, which is however not the exact BER but the approximate BER for the MIC due to the use of Gaussian approximation in the analysis.

Next, we will study the effect of the channel estimation error on the performance of the MIC.

**Effect of channel estimation error**

We assume that the variance of the channel estimation error in (11) is the same for all $l$ and $k$ and can be denoted by $\sigma_w^2$.

The bit error rate estimated from the simulation for the MIC in 3-user system with SNR=20dB and $N$=31 over 2-path Rayleigh fading channels is plotted versus $\sigma_w^2$ in Fig.11. All users are considered with equal power. It can be seen that when the variance of the channel estimation noise is less than $10^{-2}$, both the MIC (new) and the MIC (old) with $i > 0$ can still provide significant performance improvement over the conventional detector (MIC-0), in which no interference cancellation scheme is used. As the variance of the estimation noise increases, the performance difference would become small. Nevertheless, it is shown in Fig.11 that even in the presence of the estimation noise the new MIC still outperforms the old one (MIC (old)).

In Fig.12, we compare the analytical and simulation results on the bit error rates of the MIC (new) versus $\sigma_w^2$ in 3-user system with SNR=20dB and $N$=31 over 2-path Rayleigh fading channels. We are still considering the equal power for all users. The BERs of the MIC-0,1,2 are obtained via simulation, while the upper and lower bounds for the MIC-0 are evaluated respectively via (52) and (53). The upper and lower bounds for the MIC-1,2 are obtained via (56) and (57), respectively. It can be seen that the simulation results of the MIC-0,1,2 are well upper and lower bounded by the analytical ones.

Further simulation results on the BER of the MIC versus the number of users ($K$) at SNR=20dB over 2-path Rayleigh fading channels are plotted in Fig.13 and the corresponding upper and lower bounds for the MIC (new) shown in Fig.14. In both figures, the normalized variance of the channel estimation noise ($\sigma_w^2$) is set to $10^{-2}$ and all users are with equal power. It can be seen from Fig.13 that as $K$ increases, the performances of both the MIC-1 (new) and the MIC-1(old) are degraded. Also, a slight performance degradation occurs for the MIC-2. This phenomenon is due to the disturbance of the channel estimation error. The more users, the more residual interference even if all the tentative decisions in the previous stage are correct. Further, the results show that in the case of imperfect channel knowledge, the MIC (new) still performs better than the MIC (old). In particular, if we set the BER=$10^{-3}$ as an acceptable performance level, by using the old MIC-1 and 2, the system can only accommodate 7 and 9 active users, respectively. In contrast, by using the new MIC, the system can tolerate 9 active users in the MIC-1 and at least 12 users in the MIC-2. From Fig.14, it can be seen that the simulation results are well upper and lower bounded by the analytical ones.

# 6 Conclusions

This report shows that the multistage interference cancellation (MIC) together with the Rake receiver can provide satisfactory performance in QPSK asynchronous DS/CDMA system over multipath fading channels. By subtracting the partial SI rather than the total SI, the performance of the new MIC is shown superior to that of the conventional MIC and close to the ideal performance of the single-user system. The effect of the channel estimation noise on the performance of the MIC is also studied. Analysis and simulation illustrate that in the case of a channel estimation error, performance degradation occurs in both the MIC (new) and the MIC (old). However, the new MIC still conducts better than the conventional one (MIC (old)).

# 1 Evaluation of the CF of Re$\{Xe^{j\gamma}\}$ in (43)

From (41), Re$\{Xe^{j\gamma}\}$ can be written as

$$\mathrm{Re}\{Xe^{j\gamma}\} = \frac{1}{2}\sum_{q=1}^{L_u}\left\{Y_{1,q}^{*}Y_{2,q} + Y_{1,q}Y_{2,q}^{*}\right\} \tag{59}$$

where the superscript $'*'$ denotes the complex conjugate, $Y_{1,q} = c_q + g_q$, and $Y_{2,q} = (c_q\sqrt{2\rho_u} + z_q)e^{j\gamma}$, where $c_q$, $g_q$, and $z_q$ are the $q$-th elements in the vectors $C$, $G$, and $Z$, respectively.

We assume that $\frac{1}{2}E\{GG^H\} = \lambda^{(G)}\mathbf{I}$. Thus, conditioning on the channel parameter $C$, $Y_{1,q}$ and $Y_{2,q}$ form a pair of complex-valued Gaussian random variables. For different $q$, they are statistically independent but the pairs of $\{Y_{1,q}, Y_{2,q}\}$ are not identically distributed. If they are, the results in [1, Appendix C] for the error probability in the presence of the estimation error can be directly applied.

By eq.B-5 of [1], the CF of Re$\{Xe^{j\gamma}\}$ conditioned on $\{c_q\}$, denoted by $\Phi_\gamma(\omega|C)$, can be written as

$$\Phi_\gamma(\omega|C) = \prod_{q=1}^{L_u} \frac{\mu^2}{\omega^2+\mu^2} exp\left\{\frac{\mu^2}{\omega^2+\mu^2}\left[-\frac{\omega^2}{2}(\lambda^{(Z)}+2\rho_u\lambda^{(G)}) + j\omega\sqrt{2\rho_u}cos(\gamma)\right]|c_q|^2\right\} \quad (60)$$

where $\lambda^{(Z)}$ and $\lambda^{(G)}$ are the variances of $z_q$ and $g_q$, respectively, and $\mu$=$1/\sqrt{\lambda^{(Z)}\lambda^{(G)}}$.

In (60), $c_q$ is Gaussian distributed with zero mean and variance $\sigma_q^2$. Thus, $|c_q|^2$ is Rayleigh distributed. Averaging $\Phi_\gamma(\omega|C)$ over $\{|c_q|^2, q = 1, 2, ..., L_u\}$, it yields $\Phi_\gamma(\omega)$ as shown in (43).

# 2 Evaluation of $\mathrm{R}_F(0)$

Note that $\mathbf{R}_F(0)$ is the covariance matrix of $F(0)$=$\mathbf{Q}_\beta^H\Lambda_s^{-\frac{1}{2}}\mathbf{Q}_s^H[\underline{Si}_n^{(u)} + \underline{M}_n^{(u)}]$, and given by

$$\mathbf{R}_F(0) = \mathbf{Q}_\beta^H\Lambda_s^{-\frac{1}{2}}\mathbf{Q}_s^H\left[\mathbf{R}_{Si}+\mathbf{R}_M\right]\mathbf{Q}_s\Lambda_s^{-\frac{1}{2}}\mathbf{Q}_\beta \quad (61)$$

where $\mathbf{R}_{Si}$ and $\mathbf{R}_M$ denote respectively the covariance matrices of $\underline{Si}_n^{(u)}$ and $\underline{M}_n^{(u)}$.

From (20) and (21), we have

$$\begin{aligned}
\frac{1}{2}\mathrm{E}\left\{Si_{n,q_1}^{(u)}Si_{n,q_2}^{*(u)}\right\} &= 2\rho_u \sum_{l=1,l\neq q_1,l\neq q_2}^{L_u} \frac{1}{2}\mathrm{E}\{\alpha_l^{(u)}\alpha_l^{*(u)}\}\cdot \\
&\quad \mathrm{E}\left\{\left[d_{m_1+1}e^{-j\phi_{n-m_1-1}^{(u)}}R_{u,u}(\tau'_{u,l;u,q_1}) + d_{m_1}e^{-j\phi_{n-m_1}^{(u)}}\hat{R}_{u,u}(\tau'_{u,l;u,q_1})\right]\cdot\right. \\
&\quad \left.\left[d_{m_2+1}e^{-j\phi_{n-m_2-1}^{(u)}}R_{u,u}(\tau'_{u,l;u,q_2}) + d_{m_2}e^{-j\phi_{n-m_2}^{(u)}}\hat{R}_{u,u}(\tau'_{u,l;u,q_2})\right]^*\right\} \\
&= 2\rho_u \sum_{l=1,l\neq q_1,l\neq q_2}^{L_u} \frac{1}{2}\mathrm{E}\{\alpha_l^{(u)}\alpha_l^{*(u)}\}\cdot \\
&\quad \left[d_{m_1+1}d_{m_2+1}R_{u,u}(\tau'_{u,l;u,q_1})R_{u,u}^*(\tau'_{u,l;u,q_2})\mathrm{E}\{e^{j(\phi_{n-m_2-1}^{(u)}-\phi_{n-m_1-1}^{(u)})}\}\right. \\
&\quad +d_{m_1}d_{m_2+1}\hat{R}_{u,u}(\tau'_{u,l;u,q_1})R_{u,u}^*(\tau'_{u,l;u,q_2})\mathrm{E}\{e^{j(\phi_{n-m_2-1}^{(u)}-\phi_{n-m_1}^{(u)})}\} \\
&\quad +d_{m_1+1}d_{m_2}R_{u,u}(\tau'_{u,l;u,q_1})\hat{R}_{u,u}^*(\tau'_{u,l;u,q_2})\mathrm{E}\{e^{j(\phi_{n-m_2}^{(u)}-\phi_{n-m_1-1}^{(u)})}\} \\
&\quad \left.+d_{m_1}d_{m_2}\hat{R}_{u,u}(\tau'_{u,l;u,q_1})\hat{R}_{u,u}^*(\tau'_{u,l;u,q_2})\mathrm{E}\{e^{j(\phi_{n-m_2}^{(u)}-\phi_{n-m_1}^{(u)})}\}\right]
\end{aligned} \quad (62)$$

and

$$
\begin{aligned}
\frac{1}{2}\mathrm{E}\left\{M_{n,q_1}^{(u)}M_{n,q_2}^{*(u)}\right\} &= \sum_{k=1,k\neq u}^{K} 2\rho_k \sum_{l=1}^{L_k}\frac{1}{2}\mathrm{E}\{\alpha_l^{(k)}\alpha_l^{*(k)}\}\cdot \\
&\quad \mathrm{E}\left\{\left[e^{-j\phi_{n-m_1-1}^{(k)}}R_{k,u}(\tau'_{k,l;u,q_1}) + e^{-j\phi_{n-m_1}^{(k)}}\hat{R}_{k,u}(\tau'_{k,l;u,q_1})\right]\cdot\right. \\
&\quad \left.\left[e^{-j\phi_{n-m_2-1}^{(k)}}R_{k,u}(\tau'_{k,l;u,q_2}) + e^{-j\phi_{n-m_2}^{(k)}}\hat{R}_{k,u}(\tau'_{k,l;u,q_2})\right]^*\right\} \\
&= \sum_{k=1,k\neq u}^{K} 2\rho_k \sum_{l=1}^{L_k}\frac{1}{2}\mathrm{E}\{\alpha_l^{(k)}\alpha_l^{*(k)}\}\cdot \\
&\quad \left[R_{k,u}(\tau'_{k,l;u,q_1})R_{k,u}^*(\tau'_{k,l;u,q_2})\mathrm{E}\{e^{j(\phi_{n-m_2-1}^{(k)}-\phi_{n-m_1-1}^{(k)})}\}\right. \\
&\quad +\hat{R}_{k,u}(\tau'_{k,l;u,q_1})R_{k,u}^*(\tau'_{k,l;u,q_2})\mathrm{E}\{e^{j(\phi_{n-m_2-1}^{(k)}-\phi_{n-m_1}^{(k)})}\} \\
&\quad +R_{k,u}(\tau'_{k,l;u,q_1})\hat{R}_{k,u}^*(\tau'_{k,l;u,q_2})\mathrm{E}\{e^{j(\phi_{n-m_2}^{(k)}-\phi_{n-m_1-1}^{(k)})}\} \\
&\quad \left.+\hat{R}_{k,u}(\tau'_{k,l;u,q_1})\hat{R}_{k,u}^*(\tau'_{k,l;u,q_2})\mathrm{E}\{e^{j(\phi_{n-m_2}^{(k)}-\phi_{n-m_1}^{(k)})}\}\right] \qquad (63)
\end{aligned}
$$

where $m_i$=$\lfloor(\tau_l^{(k)}-\tau_{q_i}^{(k)})/T_b\rfloor$ for $i$=1,2. The expectation involved (62) and (63) can be given by

$$
\mathrm{E}\{e^{j(\phi_{n-r_2}^{(u)}-\phi_{n-r_1}^{(u)})}\} = \begin{cases} 1, & \text{if } r_2 = r_1 \\ 0, & \text{otherwise} \end{cases} \qquad (64)
$$

where $r_1$ and $r_2$ are taken from the sets of $\{m_1, m_1+1\}$ and $\{m_2, m_2+1\}$, respectively.

# 3 Evaluation of $\mathrm{R}_F^{(up)}(i)$ and $\mathrm{R}_F^{(low)}(i)$

Generally, the covariance matrix of $F(i)$ can be denoted by

$$
\mathbf{R}_F(i) = \mathbf{Q}_\beta^H\Lambda_s^{-\frac{1}{2}}\mathbf{Q}_s^H\left[\mathbf{R}_{\tilde{S}i}(i-1)+\mathbf{R}_{\tilde{M}}(i-1)\right]\mathbf{Q}_s\Lambda_s^{-\frac{1}{2}}\mathbf{Q}_\beta \qquad (65)
$$

where $\mathbf{R}_{\tilde{S}i}(i-1)$ and $\mathbf{R}_{\tilde{M}}(i-1)$ denote respectively the covariance matrices of $\underline{\tilde{S}i}_n^{(u)}(i-1)$ and $\underline{\tilde{M}}_n^{(u)}(i-1)$.

Considering the channel estimation error for $\alpha_l^{(k)}$ in $\hat{S}i_{n,q}^{(u)}(i-1)$ and $\hat{M}_{n,q}^{(k)}(i-1)$ given by (24) and (25), we have

$$
\begin{aligned}
\tilde{S}i_{n,q}^{(u)}(i-1) &= \sqrt{2\rho_u}\sum_{l=1,l\neq q}^{L_u}\alpha_l^{(u)}\left[d_{m+1}\left(e^{-j\phi_{n-m-1}^{(u)}}-e^{-j\hat{\phi}_{n-m-1}^{(u)}(i-1)}\right)R_{u,u}(\tau'_{u,l;u,q})\right. \\
&\quad \left.+d_m\left(e^{-j\phi_{n-m}^{(u)}}-e^{-j\hat{\phi}_{n-m}^{(u)}(i-1)}\right)\hat{R}_{u,u}(\tau'_{u,l;u,q})\right] \\
&\quad -\sqrt{2\rho_u}\sum_{l=1,l\neq q}^{L_u}\Delta\alpha_l^{(u)}\left[d_{m+1}e^{-j\hat{\phi}_{n-m-1}^{(u)}(i-1)}R_{u,u}(\tau'_{u,l;u,q})\right. \\
&\quad \left.+d_m e^{-j\hat{\phi}_{n-m}^{(u)}(i-1)}\hat{R}_{u,u}(\tau'_{u,l;u,q})\right] \qquad (66)
\end{aligned}
$$

and

$$\begin{aligned}
\tilde{M}_{n,q}^{(u)}(i-1) &= \sum_{k=1,k\neq u}^{K}\sqrt{2\rho_k}\sum_{l=1}^{L_k}\alpha_l^{(k)}\left[\left(e^{-j\phi_{n-m-1}^{(k)}}-e^{-j\hat{\phi}_{n-m-1}^{(k)}(i-1)}\right)R_{k,u}(\tau'_{k,l;u,q})\right.\\
&\quad\left.+\left(e^{-j\phi_{n-m}^{(k)}}-e^{-j\hat{\phi}_{n-m}^{(k)}(i-1)}\right)\hat{R}_{k,u}(\tau'_{k,l;u,q})\right]\\
&\quad-\sum_{k=1,k\neq u}^{K}\sqrt{2\rho_k}\sum_{l=1}^{L_k}\Delta\alpha_l^{(k)}\left[e^{-j\hat{\phi}_{n-m-1}^{(k)}(i-1)}R_{k,u}(\tau'_{k,l;u,q})\right.\\
&\quad\left.+e^{-j\hat{\phi}_{n-m}^{(k)}(i-1)}\hat{R}_{k,u}(\tau'_{k,l;u,q})\right] \qquad (67)
\end{aligned}$$

As a result,

$$\begin{aligned}
\frac{1}{2}\mathrm{E}\left\{\tilde{S}i_{n,q_1}^{(u)}(i-1)\tilde{S}i_{n,q_2}^{*(u)}(i-1)\right\} &= 2\rho_u\sum_{l=1,l\neq q_1,l\neq q_2}^{L_u}\frac{1}{2}\mathrm{E}\{[\Delta\alpha_l^{(u)}][\Delta\alpha_l^{*(u)}]\}\cdot\\
&\quad\left[d_{m_1+1}d_{m_2+1}R_{u,u}(\tau'_{u,l;u,q_1})R_{u,u}^*(\tau'_{u,l;u,q_2})\hat{E}_{m_1+1,m_2+1}^{(u)}\right.\\
&\quad+d_{m_1}d_{m_2+1}\hat{R}_{u,u}(\tau'_{u,l;u,q_1})R_{u,u}^*(\tau'_{u,l;u,q_2})\hat{E}_{m_1,m_2+1}^{(u)}\\
&\quad+d_{m_1+1}d_{m_2}R_{u,u}(\tau'_{u,l;u,q_1})\hat{R}_{u,u}^*(\tau'_{u,l;u,q_2})\hat{E}_{m_1+1,m_2}^{(u)}\\
&\quad\left.+d_{m_1}d_{m_2}\hat{R}_{u,u}(\tau'_{u,l;u,q_1})\hat{R}_{u,u}^*(\tau'_{u,l;u,q_2})\hat{E}_{m_1,m_2}^{(u)}\right]\\
&\quad+2\rho_u\sum_{l=1,l\neq q_1,l\neq q_2}^{L_u}\frac{1}{2}\mathrm{E}\{\alpha_l^{(u)}\alpha_l^{*(u)}\}\cdot\\
&\quad\left[d_{m_1+1}d_{m_2+1}R_{u,u}(\tau'_{u,l;u,q_1})R_{u,u}^*(\tau'_{u,l;u,q_2})E_{m_1+1,m_2+1}^{(u)}\right.\\
&\quad+d_{m_1}d_{m_2+1}\hat{R}_{u,u}(\tau'_{u,l;u,q_1})R_{u,u}^*(\tau'_{u,l;u,q_2})E_{m_1,m_2+1}^{(u)}\\
&\quad+d_{m_1+1}d_{m_2}R_{u,u}(\tau'_{u,l;u,q_1})\hat{R}_{u,u}^*(\tau'_{u,l;u,q_2})E_{m_1+1,m_2}^{(u)}\\
&\quad\left.+d_{m_1}d_{m_2}\hat{R}_{u,u}(\tau'_{u,l;u,q_1})\hat{R}_{u,u}^*(\tau'_{u,l;u,q_2})E_{m_1,m_2}^{(u)}\right] \qquad (68)
\end{aligned}$$

and

$$\begin{aligned}
\frac{1}{2}\mathrm{E}\left\{\tilde{M}_{n,q_1}^{(u)}(i-1)\tilde{M}_{n,q_2}^{*(u)}(i-1)\right\} &= \sum_{k=1,k\neq u}^{K} 2\rho_k \sum_{l=1}^{L_k} \frac{1}{2}\mathrm{E}\{[\Delta\alpha_l^{(k)}][\Delta\alpha_l^{*(k)}]\}\cdot \\
&\Big[R_{k,u}(\tau'_{k,l;u,q_1})R^*_{k,u}(\tau'_{k,l;u,q_2})\hat{E}^{(k)}_{m_1+1,m_2+1} \\
&+\hat{R}_{k,u}(\tau'_{k,l;u,q_1})R^*_{k,u}(\tau'_{k,l;u,q_2})\hat{E}^{(k)}_{m_1,m_2+1} \\
&+R_{k,u}(\tau'_{k,l;u,q_1})\hat{R}^*_{k,u}(\tau'_{k,l;u,q_2})\hat{E}^{(k)}_{m_1+1,m_2} \\
&+\hat{R}_{k,u}(\tau'_{k,l;u,q_1})\hat{R}^*_{k,u}(\tau'_{k,l;u,q_2})\hat{E}^{(k)}_{m_1,m_2}\Big] \\
&+\sum_{k=1,k\neq u}^{K} 2\rho_k \sum_{l=1}^{L_k} \frac{1}{2}\mathrm{E}\{\alpha_l^{(k)}\alpha_l^{*(k)}\}\cdot \\
&\Big[R_{k,u}(\tau'_{k,l;u,q_1})R^*_{k,u}(\tau'_{k,l;u,q_2})E^{(k)}_{m_1+1,m_2+1} \\
&+\hat{R}_{k,u}(\tau'_{k,l;u,q_1})R^*_{k,u}(\tau'_{k,l;u,q_2})E^{(k)}_{m_1,m_2+1} \\
&+R_{k,u}(\tau'_{k,l;u,q_1})\hat{R}^*_{k,u}(\tau'_{k,l;u,q_2})E^{(k)}_{m_1+1,m_2} \\
&+\hat{R}_{k,u}(\tau'_{k,l;u,q_1})\hat{R}^*_{k,u}(\tau'_{k,l;u,q_2})E^{(k)}_{m_1,m_2}\Big] \qquad (69)
\end{aligned}$$

where $m_i$=$\lfloor(\tau_l^{(k)}-\tau_{q_i}^{(k)})/T_b\rfloor$ for $i$=1,2, $\hat{E}^{(k)}_{r_1,r_2}$ and $E^{(k)}_{r_1,r_2}$ are respectively given by

$$\hat{E}^{(k)}_{r_1,r_2} = E\{e^{j[\hat{\phi}^{(k)}_{n-r_2}(i-1)-\hat{\phi}^{(k)}_{n-r_1}(i-1)]}\} = \begin{cases} 1, & \text{if } r_2 = r_1 \\ 0, & \text{otherwise} \end{cases} \qquad (70)$$

and

$$\begin{aligned}
E^{(k)}_{r_1,r_2} &= \mathrm{E}\left\{\left[e^{-j\phi^{(k)}_{n-r_1}} - e^{-j\hat{\phi}^{(k)}_{n-r_1}(i-1)}\right]\left[e^{-j\phi^{(k)}_{n-r_2}} - e^{-j\hat{\phi}^{(k)}_{n-r_2}(i-1)}\right]^*\right\} \\
&= \begin{cases} \frac{1}{4}\sum_{p=1}^{4}\sum_{\hat{p}=1,\hat{p}\neq p}^{4} g_1(p,\hat{p}) & \text{if } r_1 = r_2 = r \\ \frac{1}{16}\sum_{p_1=1}^{4}\sum_{\hat{p}_1=1,\hat{p}_1\neq p_1}^{4}\sum_{p_2=1}^{4}\sum_{\hat{p}_2=1,\hat{p}_2\neq p_2}^{4} g_2(p_1,p_2,\hat{p}_1,\hat{p}_2) & \text{otherwise} \end{cases} \qquad (71)
\end{aligned}$$

$r_1$ and $r_2$ are taken from the sets of $\{m_1, m_1+1\}$ and $\{m_2, m_2+1\}$, respectively, and

$$g_1(p,\hat{p}) = \left[e^{-j\psi_p} - e^{-j\psi_{\hat{p}}}\right]\left[e^{-j\psi_p} - e^{-j\psi_{\hat{p}}}\right]^* P_s\left\{\hat{\phi}^{(k)}_{n-r}(i-1) = \psi_{\hat{p}} | \phi^{(k)}_{n-r} = \psi_p\right\} \qquad (72)$$

$$\begin{aligned}
g_2(p_1,p_2,\hat{p}_1,\hat{p}_2) &= \left[e^{-j\psi_{p_1}} - e^{-j\psi_{\hat{p}_1}}\right]\left[e^{-j\psi_{p_2}} - e^{-j\psi_{\hat{p}_2}}\right]^* P_s\left\{\hat{\phi}^{(k)}_{n-r_1}(i-1) = \psi_{\hat{p}_1} | \phi^{(k)}_{n-r_1} = \psi_{p_1}\right\}\cdot \\
&\quad P_s\left\{\hat{\phi}^{(k)}_{n-r_2}(i-1) = \psi_{\hat{p}_2} | \phi^{(k)}_{n-r_2} = \psi_{p_2}\right\} \qquad (73)
\end{aligned}$$

$\psi_p := 2\pi(p-1)/4$ is the possible phase shift, and $P_s\{\hat{\phi}^{(k)}_n(i-1) = \psi_{\hat{p}} | \phi^{(k)}_n = \psi_p\}$ is the symbol error probability when $\phi^{(k)}_n = \psi_p$ is transmitted while the tentative decision in the $(i-1)$-th stage is $\psi_{\hat{p}}$.

For user $k$, let $X^{(k)}(i-1)$ be the test statistic in the $(i-1)$-th stage. Thus, $P_s\{\hat{\phi}_n^{(k)}(i-1)= \psi_{\hat{p}}|\phi_n^{(k)}= \psi_p\}$= Pr$\{X^{(k)}(i-1)e^{j\psi_p} \in R_t\}$= $A_t$, where $R_t$ is region that the vector $e^{j(\hat{\phi}_n^{(k)}(i-1)-\phi_n^{(k)})}$ falls in (see [31, 34]). Following the approach in [31], we have

$$\begin{aligned} A_1 &= \mathcal{F}(\gamma = -\pi/4)\mathcal{F}(\gamma = -3\pi/4) \\ A_2 &= \mathcal{F}(\gamma = -\pi/4)\mathcal{F}(\gamma = \pi/4) \\ A_3 &= \mathcal{F}(\gamma = \pi/4)\mathcal{F}(\gamma = 3\pi/4) \end{aligned} \tag{74}$$

where $\mathcal{F}(\gamma) :=$ Pr$\{X^{(k)}(i-1)e^{j\psi_p}e^{j\gamma} < 0\}$.

When the bit error rate is irrelevant or weakly dependent on $\psi_p$, we may evaluate (74) by setting $\psi_p$=0 and we have

$$\begin{aligned} \mathcal{F}(\gamma = \pi/4) &= \mathcal{F}(\gamma = -\pi/4) \\ \mathcal{F}(\gamma = -3\pi/4) &= \mathcal{F}(\gamma = 3\pi/4) = 1 - \mathcal{F}(\gamma = -\pi/4) \end{aligned} \tag{75}$$

where $\mathcal{F}(\gamma = -\pi/4)$ is the bit error rate of user $k$ in the $(i-1)$-th stage. One can readily check that by substituting (74) and (75) into (38), we have $P_b = \mathcal{F}(\gamma = -\pi/4)$.

As previously mentioned, due to the correlated residual interference, the exact evaluation of $\mathcal{F}(\gamma = -\pi/4)$ is quite difficult and thus the upper and lower bounds in $(i-1)$-th stage denoted by $P_b^{(up)}(i-1)$ and $P_b^{(low)}(i-1)$, respectively, are derived in Section 4.2. Furthermore, by using the Gaussian approximation for the interference, these upper and lower bounds on the BER are irrelevant to the transmitted symbols. Therefore, instead of computing the exact $\mathbf{R}_F(i)$, we may compute $\mathbf{R}_F^{(up)}(i)$ and $\mathbf{R}_F^{(low)}(i)$ relying on $P_b^{(up)}(i-1)$ and $P_b^{(low)}(i-1)$, respectively. In particular, by letting $\mathcal{F}(\gamma = -\pi/4)$=$P_b^{(up)}(i-1)$ in (75) for all users, the resulting $\mathbf{R}_F(i)$ is referred to as $\mathbf{R}_F^{(up)}(i)$. On the other hand, letting $\mathcal{F}(\gamma = -\pi/4)$=$P_b^{(low)}(i-1)$ for all users, we obtain $\mathbf{R}_F^{(low)}$.

# Bibliography


[1] J. G. Proakis, *Digital communications*. New York: McGraw-Hill, 1995.

[2] R. L. Pickholtz, L. B. Milstein, and D. L. Schilling, "Spread spectrum for mobile communications," *IEEE Trans. Vehi. Tech.*, vol. VT-40, pp. 313–321, May 1991.

[3] W. C. Y. Lee, "Overview of cellular CDMA," *IEEE Trans. Vehi. Tech.*, vol. VT-40, pp. 291–302, May 1991.

[4] S. Verdu, "Minimum probability of error for asynchronous Gaussian multiple access channels," *IEEE Trans. Inform. Theo.*, vol. IT-32, pp. 85–96, Jan. 1986.

[5] R. Lupas and S. Verdu, "Near-far resistance of multiuser detectors in asynchronous channels," *IEEE Trans. Commun.*, vol. COM-38, pp. 496–508, Sep. 1990.

[6] M. K. Varanasi and B. Aazhang, "Multistage detection in asynchronous code-division multiple-access communications," *IEEE Trans. Commun.*, vol. COM-38, pp. 509–519, April 1990.

[7] T. Miyajima, T. Hasegawa, and M. Haneishi, "On the multiuser detection using a neural network in code-division multiple-access communications," *IEICE Trans. Commun.*, vol. E76-B, pp. 961–968, Aug. 1993.

[8] M. K. Varanasi, "Noncoherent detection in asynchronous multiuser channels," *IEEE Trans. Inform. Theo.*, vol. IT-39, pp. 157–176, Jan. 1993.

[9] P. Patel and J. Holtzman, "Analysis of a simple successive interference cancellation scheme in a DS/CDMA system," *IEEE J. Select. Areas Commun.*, vol. SAC-12, pp. 796–807, June 1994.

[10] A. Kajiwara and M. Nakagawa, "Microcellular cdma system with a linear multiuser interference canceler," *IEEE J. Select. Areas Commun.*, vol. SAC-12, pp. 605–611, May 1994.

[11] L. B. Nelson and H. V. Poor, "Iterative multiuser receivers for CDMA channels: an EM-based approach," *IEEE Trans. Commun.*, vol. COM-44, pp. 1700–1710, Dec 1996.

[12] U. Madhow and M. L. Honig, "MMSE interference suppression for direct sequence spread spectrum CDMA," *IEEE Trans. Commun.*, vol. COM-42, pp. 3178–3188, Dec. 1994.

[13] U. Mitra and H. V. Poor, "Adaptive receiver algorithms for near-far resistant CDMA," *IEEE Trans. Commun.*, vol. COM-43, pp. 1713–1724, Feb./Mar./April 1995.

[14] S. Verdu, "Adaptive multiuser detection," in *Proc. IEEE 3rd Int. Symp. Spread Spectrum Tech. and Appl., ISSSTA'94*, (Oulu, Finland), pp. 43–50, July 1994.

[15] D. Chen and S. Roy, "An adaptive multiuser receiver for CDMA systems," *IEEE J. Select. Areas Commun.*, vol. SAC-12, pp. 808–816, June 1994.

[16] U. Fawer and B. Aazhang, "A multiuser receiver for code division multiple access communication over multipath channels," *IEEE Trans. Commun.*, vol. COM-43, pp. 1556–1565, Feb./Mar./April 1995.

[17] Z. Zvonar, "Combined multiuser detection and diversity reception for wireless CDMA systems," *IEEE Trans. Vehi. Tech.*, vol. VT-45, pp. 205–211, Feb. 1996.

[18] A. E. Brand and A. H. Aghvami, "Performance of a joint CDMA/PRMA propocol for mixed voice/data transmission for third generation mobile communications," *IEEE J. Select. Areas Commun.*, vol. SAC-14, pp. 1698–1707, Dec. 1996.

[19] W. B. Yang and E. Geraniotis, "Admission policies for integrated voice and data traffic in CDMA packet radio networks," *IEEE J. Select. Areas Commun.*, vol. SAC-12, pp. 654–664, May 1994.

[20] Y. C. Yoon, R. Kohno, and H. Imai, "A spread-spectrum multiaccess system with cochannel interference cancellation for multipath fading channels," *IEEE J. Select. Areas Commun.*, vol. SAC-11, pp. 1067–1075, Sept. 1993.

[21] A. L. C. Hui and K. B. Letaief, "Successive interference cancellation for multiuser asynchronous DS/CDMA detectors in multipath fading links," *IEEE Trans. Commun.*, vol. COM-46, pp. 384–391, Mar. 1998.

[22] R. L. Peterson, R. E. Ziemer, and D. E. Borth, *Introduction to spread spectrum communications*. London: Prentice-Hall, Inc., 1995.

[23] G. Q. Xue, *Performance investigation and simulation of cellular CDMA system*. PhD thesis, Southeast Univ., Nanjing, P. R. China, Jan. 1996.

[24] G. D. Boudreau, D. D. Falconer, and S. A. Mahmoud, "A comparison of trellis coded versus convolutionally coded spread spectrum multiple-access system," *IEEE J. Select. Areas Commun.*, vol. SAC-8, pp. 628–640, May 1990.

[25] R. A. Iltis and L. Mailaender, "An adaptive multiuser detector with joint amplitude and delay estimation," *IEEE J. Select. Areas Commun.*, vol. SAC-12, pp. 774–785, June 1994.

[26] R. A. Iltis, "A GLRT-based spread spectrum receiver for joint channel estimation and interference suppression," *IEEE Trans. Commun.*, vol. COM-37, pp. 277–288, Mar. 1989.

[27] B. D. O. Anderson and J. B. Moore, *Optimal filtering*. Prentice-hall information and system sciences series, N. J.: Englewood Cliffs, 1979.

[28] M. B. Pursley, "Performance evaluation for phase-coded spread-spectrum multiple access communication - part I: system analysis," *IEEE Trans. Commun.*, vol. COM-25, pp. 795–799, Aug. 1977.

[29] S. Haykin, *Adaptive filter theory*. Prentice Hall information and system sciences series, New Jersey: Prentice-Hall Int., 3rd ed., 1996.

[30] A. Papoulis, *Probability, random variables, and stochastic processes*. New York: McGraw-Hill, 1991.

[31] P. Y. Kam, "Bit error probability of MDPSK over the non-selective Rayleigh fading channels with diversity reception," *IEEE Trans. Commun.*, vol. COM-39, pp. 220–224, Feb. 1991.

[32] M. Schwartz, W. R. Bennett, and S. Stein, *Communication systems and techniques*. New York: McGraw-Hill, 1966.

[33] J. F. Weng, *Performance of two-stage nonlinear detector in DS/CDMA system with impulse noise*. PhD thesis, City Univ. of Hong Kong, Hong Kong, Aug. 1997.

[34] P. J. Lee, "Computation of the bit error rate of coherent M-ary PSK with Gray code bit mapping," *IEEE Trans. Commun.*, vol. COM-34, pp. 488–491, May 1986.

[35] M. B. Pursley and H. F. A. Roefs, "Numerical evaluation of correlation parameters for optimal phases of binary shift-register sequences," *IEEE Trans. Commun.*, vol. COM-27, pp. 1597–1604, Oct. 1979.

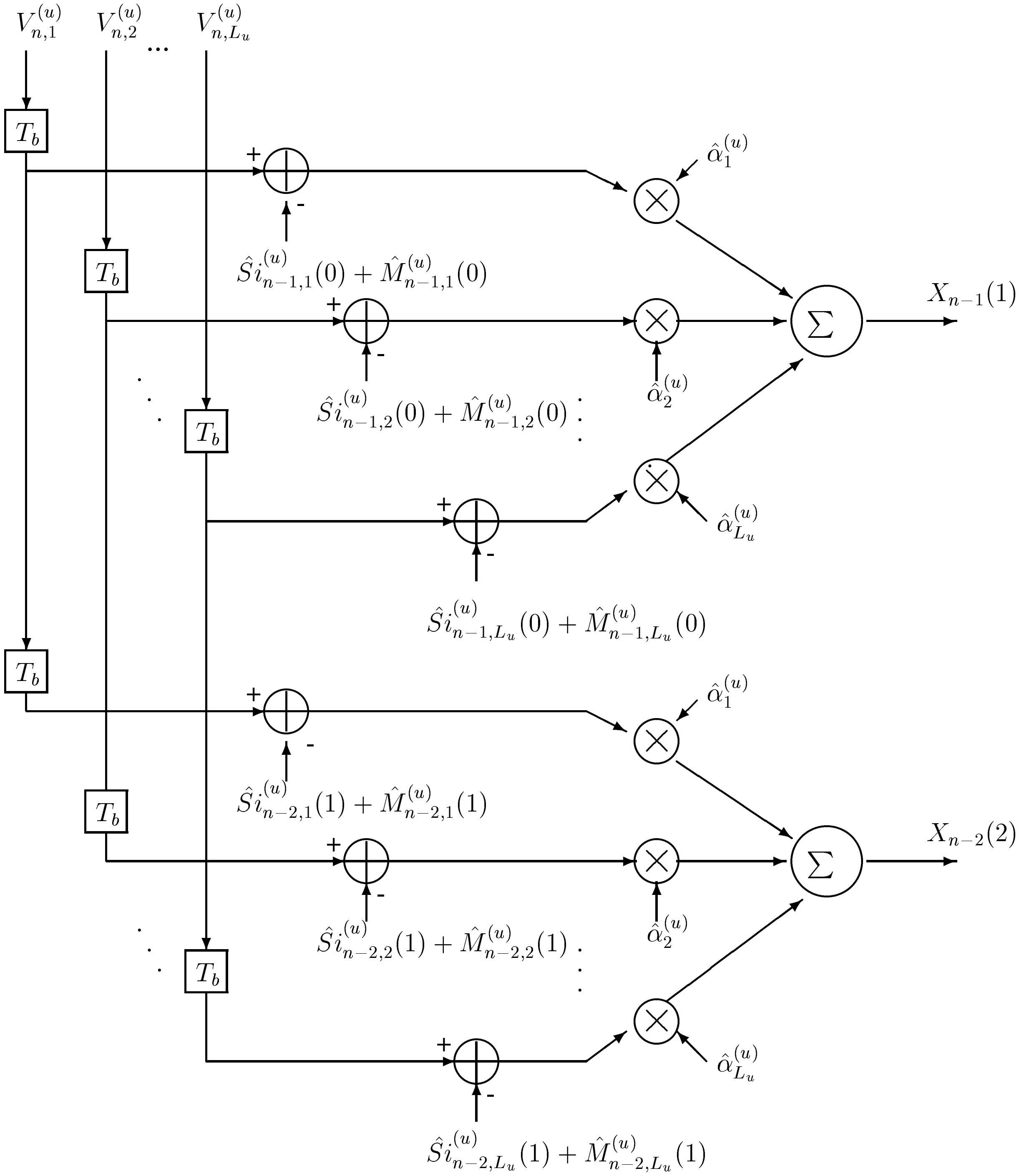


Fig. 4: New two stage MIC for user $u$

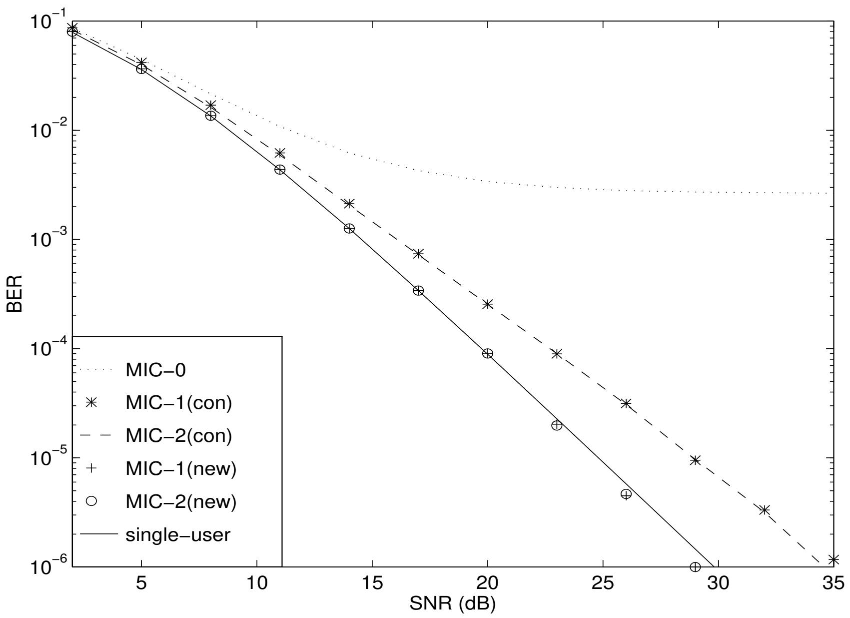


Fig. 5: Simulated bit error rates of the MIC versus SNR in 3-user system with $N$=31 over 2-path Rayleigh fading channels. All users are with equal power. MIC-0: 0-stage MIC; MIC-1: 1-stage MIC; MIC-2: 2-stage MIC.

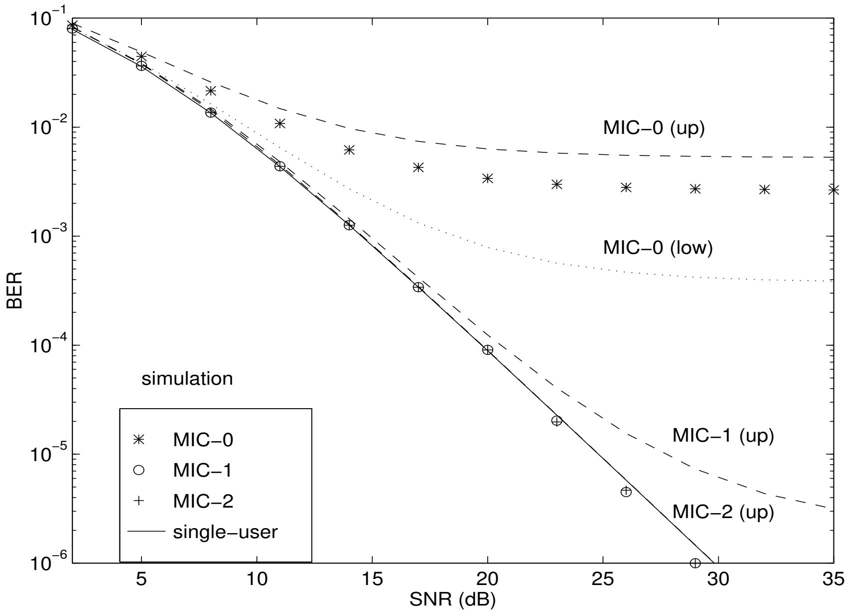


Fig. 6: Analytical and simulation results on the bit error rates of the MIC (new) versus SNR in 3-user system with $N$=31 over 2-path Rayleigh fading channels. All users are with equal power. MIC-0: 0-stage MIC; MIC-1: 1-stage MIC; MIC-2: 2-stage MIC. Dashed lines: analytical upper bound, dotted line: analytical lower bound.

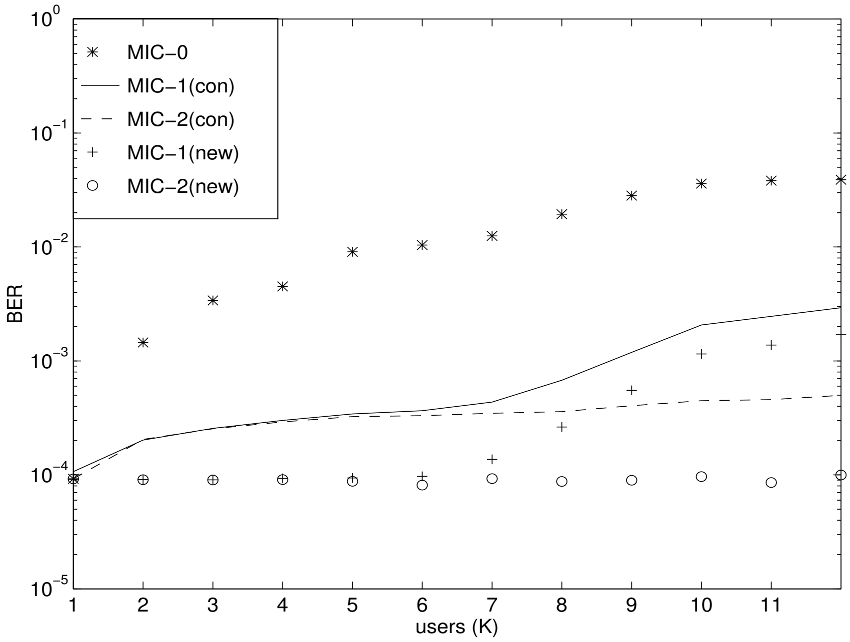


Fig. 7: Simulated bit error rates of the MIC versus the number of users ($K$) at SNR=20dB and $N$=31 over 2-path Rayleigh fading channels. All users are with equal power. MIC-0: 0-stage MIC; MIC-1: 1-stage MIC; MIC-2: 2-stage MIC.

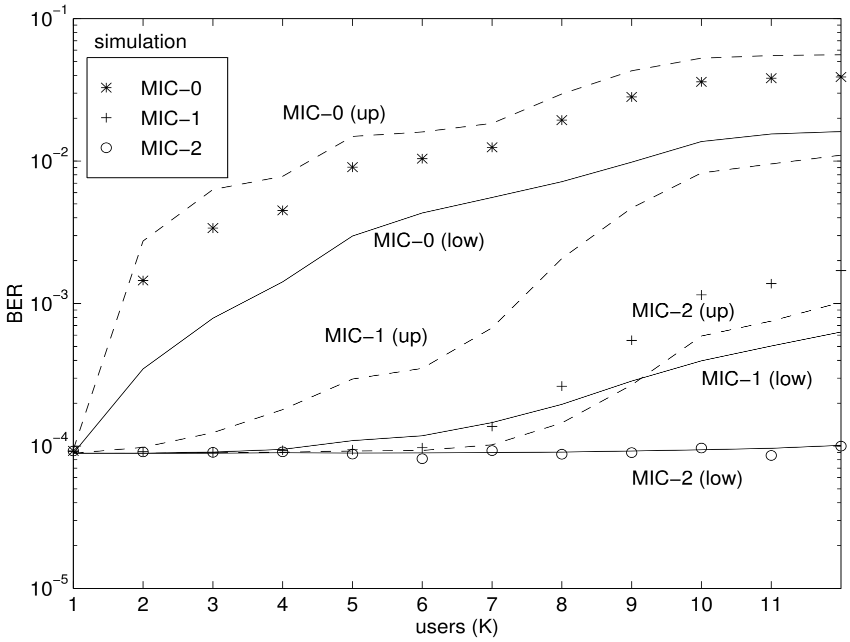


Fig. 8: Analytical and simulation results on the bit error rates of the MIC (new) versus the number of users ($K$) at SNR=20dB and $N$=31 over 2-path Rayleigh fading channels. All users are with equal power. MIC-0: 0-stage MIC; MIC-1: 1-stage MIC; MIC-2: 2-stage MIC. Dashed lines: analytical upper bound, solid lines: analytical lower bound.

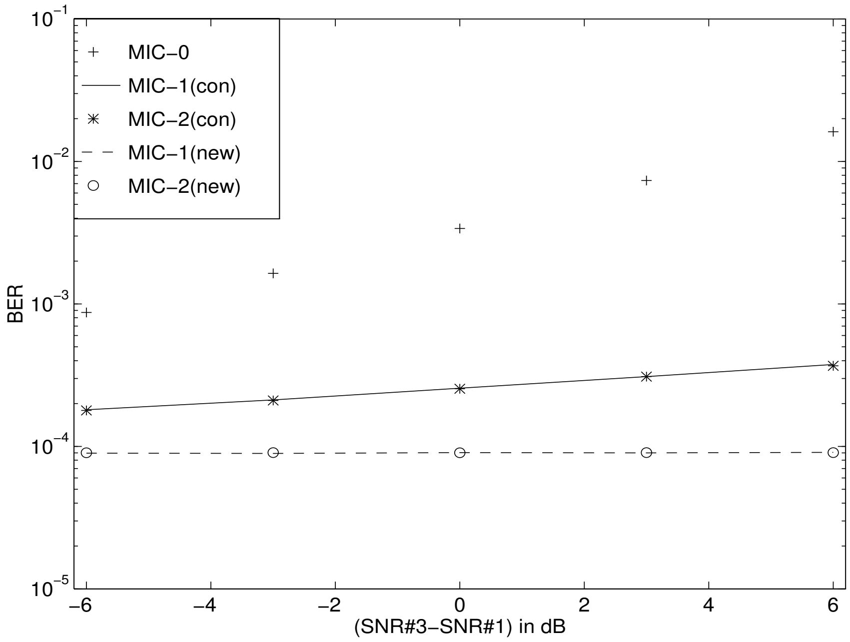


Fig. 9: Simulated bit error rates of the MIC versus SNR#3-SNR#1 dB in 3-user system with SNR#1=20dB and $N$=31 over 2-path Rayleigh fading channels. SNR#2=(SNR#3+SNR#1)/2dB. MIC-0: 0-stage MIC; MIC-1: 1-stage MIC; MIC-2: 2-stage MIC.

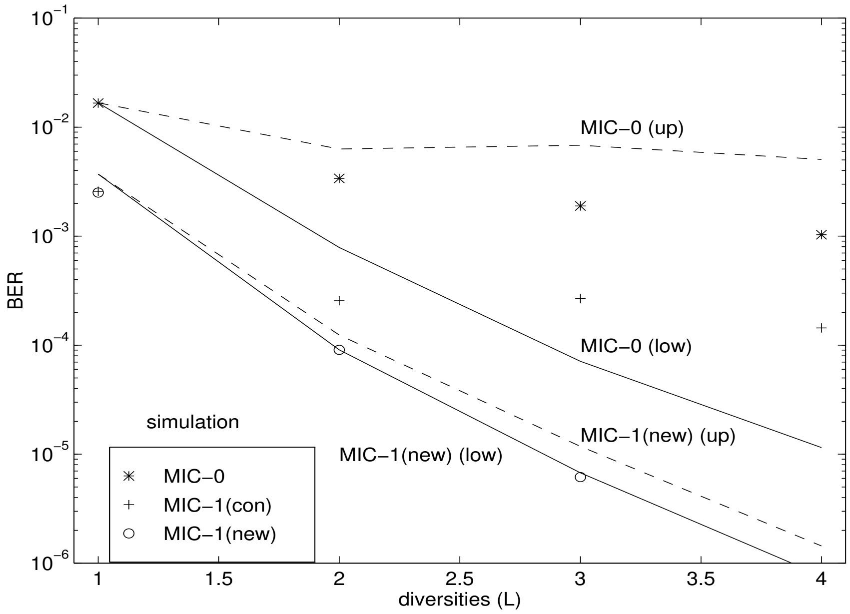


Fig. 10: Analytical and simulated bit error rates of the MIC versus the number of diversities ($L$) in 3-user system with SNR=20dB and $N$=31 over multipath Rayleigh fading channels. All users are with equal power. MIC-0: 0-stage MIC; MIC-1: 1-stage MIC. Dashed lines: analytical upper bound, solid lines: analytical lower bound.

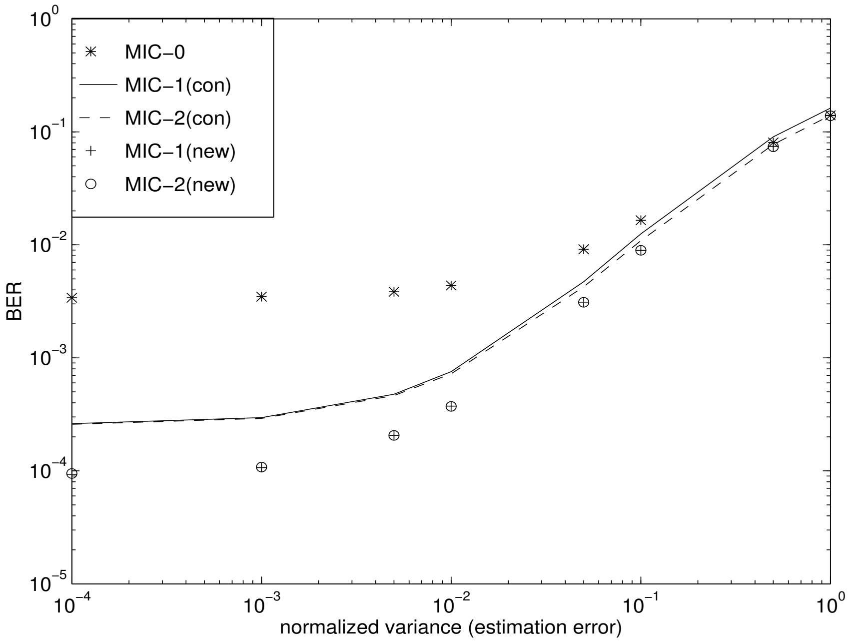


Fig. 11: Simulated bit error rates of the MIC versus the variance of the estimation error in 3-user system with SNR=20dB and $N$=31 over 2-path Rayleigh fading channels. All users are with equal power. MIC-0: 0-stage MIC; MIC-1: 1-stage MIC; MIC-2: 2-stage MIC.

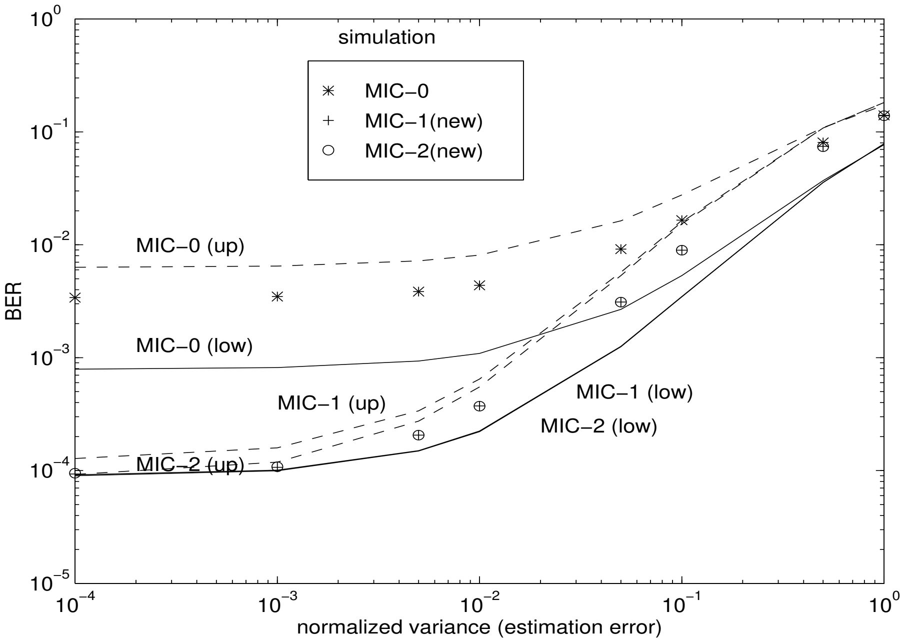


Fig. 12: Analytical and simulation results on the bit error rates of the MIC (new) versus the variance of the estimation error in 3-user system with SNR=20dB and $N$=31 over 2-path Rayleigh fading channels. All users are with equal power. MIC-0: 0-stage MIC; MIC-1: 1-stage MIC; MIC-2: 2-stage MIC. Dashed lines: upper bound, solid lines: lower bound.

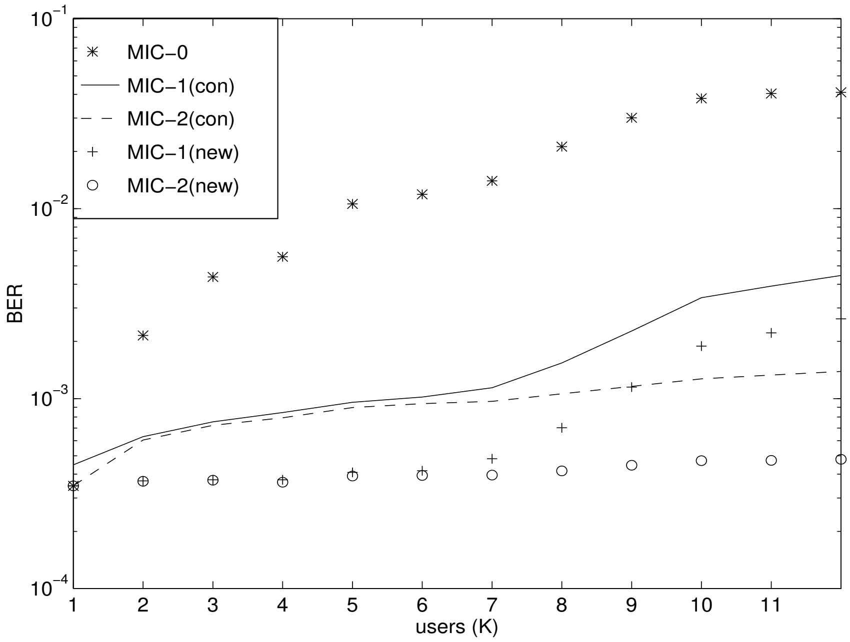


Fig. 13: Simulated bit error rates of the MIC versus the number of users ($K$) in multi-user system with SNR=20dB and $N$=31 over 2-path Rayleigh fading channels. All users are with equal power. $\sigma_w^2 = 10^{-2}$. MIC-0: 0-stage MIC; MIC-1: 1-stage MIC; MIC-2: 2-stage MIC.

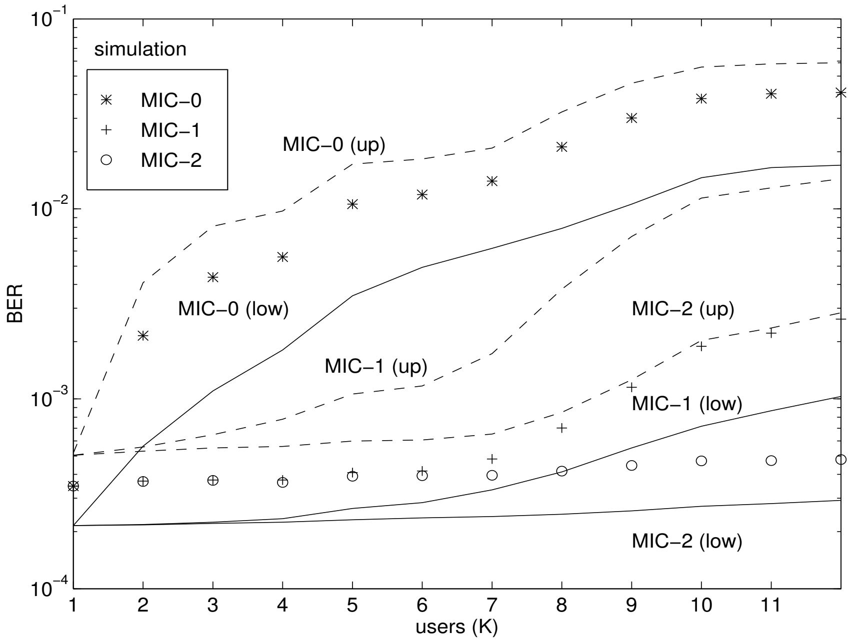


Fig. 14: Analytical and simulation results on bit error rates of the MIC (new) versus the number of users ($K$) in multi-user system with SNR=20dB and $N$=31 over 2-path Rayleigh fading channels. All users are with equal power. $\sigma_w^2 = 10^{-2}$. MIC-0: 0-stage MIC; MIC-1: 1-stage MIC; MIC-2: 2-stage MIC. Dashed lines: analytical upper bound, solid lines: analytical lower bound.